geosciences

MDPI

Article

Transgressive Architecture of Coastal Barrier Systems in the Ofanto Incised Valley and Its Surrounding Shelf in Response to Stepped Sea-Level Rise

Vincenzo De Santis *, Massimo Caldara and Luigi Pennetta

Department of Earth and Environmental Science, University of Bari, 70125 Bari, Italy; massimoangelo.caldara@uniba.it (M.C.); luigi.pennetta@uniba.it (L.P.)

* Correspondence: vincenzo.desantis@uniba.it

Received: 20 October 2020; Accepted: 7 December 2020; Published: 10 December 2020

check for updates

Abstract: Coastal deposits/barriers react to sea-level rise through rollover or overstepping. Preserved coastal deposits/barriers allow us to examine coastal responses to sea-level rise, an important aspect within the context of climate change. This study identifies the Ofanto incised valley and examines the possible factors that caused the considerable difference in shape between this valley and adjacent valleys: the Carapelle and Cervaro incised valley and Manfredonia incised valley. In addition, this study assesses the response of transgressive units to stepped sea-level rise with a focus on the evolution of palaeo-barriers/shorelines on the continental shelf and within the infill of Ofanto incised valley. We identified the traces of two slowstands in sea-level rise: the first, short-lived at a centennial scale, interrupted Meltwater Pulse 1A; the second is referable to part of Bølling-Allerød and Younger Dryas. During these two slowstands, two barrier-shoreface/estuarine-backbarrier systems formed. Meltwater Pulse 1A and Meltwater Pulse 1B led to overstepping and partial preservation of these systems in the form of aligned topographic highs. The second slowstand gave rise to continuous landward backstepping of the coastal barrier system; during the following Meltwater Pulse 1B (MWP-1B), landward rollover of the coeval barrier/backbarrier system occurred.

Keywords: coastal barrier; continuous backstepping pattern; incised valley; sapropel S1; stepped sea-level rise

1. Introduction

Rollover and overstepping are the two main responses of coastal barriers to sea-level rise [1]. Rollover is dominant and consists of a continuous landward migration of the barrier systems, with almost complete reworking of shoreface and barrier deposits [2]. During rollover, coastal deposits/barriers maintain their volume [3]. Overstepping consists of in place drowning of coastal deposits/barriers [3]; thus, they can be preserved as relict features on the seafloor. When coastal deposits/barriers are overstepped, the degree of their preservation depends on their resistance to wave ravinement processes [4,5]. Overstepping and partial preservation of coastal deposits/barriers has been typically attributed to rapid sea-level rise, such as that occurred during meltwater pulses [6], under particularly favourable circumstances: these include early cementation (beachrock and aeolianite formation) [7] or gravel and boulder barrier formation [2]. According to Pretorius et al. [8], coastal deposits/barriers, coupled with incised valley deposits, provide useful information on the evolution of coastal systems during transgression and provide important evidence for the relative balance between postglacial rises in sea level and the available sediment [9,10]. As the incised valley fill is also conditioned by the shape of valleys, it is important to investigate the factors that drive the valley geometry, the principals among which are the rate and magnitude of the base-level fall, shelf-break depth, tectonics, climate, and drainage-basin area [11].

According to Maselli et al. [12,13], Trincardi et al. [14], and Bernè et al. [15], the geometrical complexity of the sedimentary bodies belonging to the last transgressive sedimentary succession (transgressive systems tract, TST) on the Mediterranean clastic continental shelves recorded the impact of several climatic events.

In this study, we describe the incised valley of the Ofanto River, for the first time in its entirety, and the formation and landward migration of transgressive units, some of which contain coastal barriers, during the last post-marine isotope stage (MIS) 2 transgression. These transgressive units infilled the Ofanto valley and/or deposited on the surrounding continental shelf. The aim of this study is to provide an example of how coastal depositional environments migrate landward as a response to stepped rises in sea level. We also propose to discuss the causes that led to the formation of three very different incised valleys (two narrow and deep, one wide and shallow) a few kilometres away from each other. Finally, we propose a model of the stratigraphic architecture of transgressive deposits.

2. Regional Setting

The Manfredonia Gulf is the offshore continuation of the Tavoliere di Puglia Plain, the second largest plain in Italy, characterised by Quaternary marine and alluvial terraces [16–21] which, however, are widespread along the entire Apulian coast [22,23].

The Gulf is characterised by a very gently sloping sea bottom toward the east [24]. Currently, the marine current affecting the Manfredonia Gulf is characterised by a branch of the western Adriatic current that descends from the Gargano head and approaches the coastline at the Ofanto delta. From here, a branch of the littoral drift trends NW along the Gulf coast [25]. However, in the past, up to ca. 4.5–5.5 ka cal. BP, the drift current flowed in the opposite direction [26].

The coastal area of the Manfredonia Gulf is affected by subsidence, with a rate of 0.21 mm/year between marine isotope stage (MIS) 5.5 and the present day [18] and a rate of 0.11 mm/year between ca. 9 ka cal. BP and the present day [27]

In the Gulf, many authors [28–32] recognised the lowstand surface of subaerial exposure (LSSE) as an extensive regional unconformity formed during the last glacial maximum. The Manfredonia Incised Valley (MIV; Figure 1) cuts into the LSSE and is a sinuous valley more than 60 km long with a W–E orientation from the inner shelf to the mid-outer shelf. On the LSSE, the TST and the highstand system tract (HST) were deposited from the beginning of the last sea-level rise.

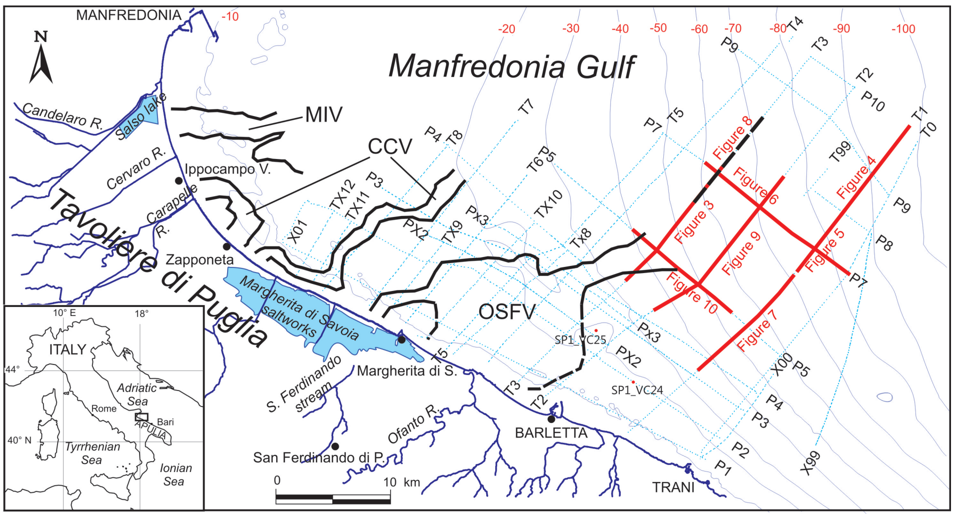

Figure 1. Study area with seismic profiles acquired in the surveys 2016–2017 (cyan); the thick black lines indicates the edges of Manfredonia incised valley (MIV, from [32]), Carapelle and Cervaro valley (CCV, from [27,32]), and Ofanto San Ferdinando valley (OSFV, from [27]). Sea bottom contour lines are also reported. The red or black dashed parts of the seismic profiles correspond to the sections reported in the figures indicated.

In the innermost area of the Manfredonia Gulf, De Santis et al. [27] recognised two erosive landforms that are incised on the surface of subaerial exposure (ES1). The first landform (the Carapelle and Cervaro valley, CCV; Figure 1) can be correlated with the current Carapelle and Cervaro streams. The second landform (the Ofanto–San Ferdinando valley, OSFV; Figure 1) can be correlated with the current Ofanto River and, subordinately, with its tributary San Ferdinando stream. De Santis et al. [27] recognised six seismic facies which are reported synthetically in Table 1, and seven unconformity-bounded seismic units (UBSUs) that buried the ES1 and/or infilled CCV and OSFV.

Table 1. Simplified sketch and short description of seismic facies recognised within the unconformity-bounded seismic units (UBSUs) belonging to the transgressive systems tract (TST) in the Manfredonia Gulf area.

Seismic Facies	
1 	Description: always present within the incised valleys, on the ES1; characterised by a high amplitude downlapping reflector or reflectors with concave and convex or wavy shapes; frequent changes are present in the immersion of the reflectors; the lateral continuity is low-moderate.
	Interpretation: fluvial lag; deposition under high-energy riverine conditions
2a 	Description: chaotic, nonsymmetrical internal configuration with reflectors of low or very low amplitude and low lateral continuity, with a V and Λ shape, or undulating, concave and convex. From offshore to onshore, a transition between facies 2 and facies 3 is often observed
	Interpretation: predominantly siliciclastic sandy deposit rich in coarse bioclasts, with a minor content of silt and/or clay, as the expression of high-energy coastal sediments (beach/shoreface/barrier (bsb))
2b 	Description: sigmoidal and/or clinoform reflectors with moderate–high amplitudes and medium–high lateral continuity, which alternate with low amplitude reflectors or with chaotic and nonsymmetrical packages, all inclined landward. Not present in the seismic profiles shown in this article
	Interpretation: beach/shoreface/barrier (bsb) deposit within a transgressive barrier or spit that migrated landward by wave erosion and overwashing
3 	Description: medium amplitude, plane-parallel reflectors with medium lateral continuity; alternatively, reflectors are weakly undulating with low lateral continuity. Often facies 2 transitions landwards to facies 3
	Interpretation: low energy, backbarrier deposit (perhaps a semienclosed bay/microtidal estuarine lagoon) behind a coastal barrier
4 	Description: medium- to high amplitude, medium-high lateral continuity wavy, concave or convex reflectors alternating with plane-parallel reflectors. In some cases, facies 2 transitions landward into facies 4
	Interpretation: open backbarrier (bay/microtidal estuarine lagoon), probably of silty nature. Presence of currents and channels, which create a moderate energy environment. The wavy undulations which characterise this facies can be interpreted in some cases as channel features, in other cases as deformation of the backbarrier bottom due to waves or currents
5 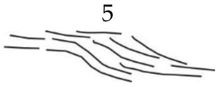	Description: medium amplitude and medium lateral continuity reflectors, with the presence of a topset, foreset and bottomset
	Interpretation: prograding deltaic body
6 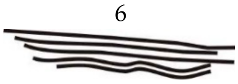	Description: medium- to high amplitude reflectors with the maximum observed lateral continuity, onlapping onto inclined substrate and/or draping over uneven substrate. Reflectors are gently seaward-inclined or subhorizontal
	Interpretation: lower shoreface/offshore, probably silty-clay deposit, related to the end of wave action on the sea bottom

In particular, in the most landward sector of the CCV, two UBSUs can be interpreted as many barrier/spit-backbarrier systems; also in the OSFV, two UBSUs can be interpreted as many beach/spit-backbarrier systems arranged in a landward backstepping pattern [33], which De Santis et al. [27] redefined as "continuous". The phase that contributed most to the creation and preservation of coastal barrier systems within the infill of the landward sector of CCV and within the infill of OSFV is coeval with the formation of sapropel S1a in the Mediterranean [27].

In the central Adriatic, the internal geometry of the transgressive system tract (TST) appears to be constituted by three main units [13,34]: the lower TST, middle TST and upper TST units, bounded by two erosive regional surfaces, S1 and S2, which have been generated by reduced sediment input and enhanced marine reworking because of Meltwater Pulses 1A and 1B (MWP-1A and MWP-1B), respectively. The lower TST unit records the sea-level rise between −120 m and −95 m, the middle TST unit between −95 m and −60 m, and the upper TST unit between −60 m and the position of the shoreline that was reached at the time of maximum marine ingression (5.5 ka cal. BP; [30,35–37]). In particular, the middle TST unit recorded a phase of intense sediment supply and sea-level stillstand (or possibly fall), attributed to the Younger Dryas cold reversal [13], which generated another regional erosional surface (Si) within the middle TST, This feature is consistent with the evidence of a Younger Dryas shoreline deposit at a depth of ca −75 m.

Within the middle TST, Pellegrini et al. [38] document the so-called Paleo Gargano Compound Delta, formed offshore the modern Gargano Promontory (southern Adriatic Sea), which is a deltaic system where both delta front sands and related fine-grained subaqueous progradations have been preserved. The Paleo Gargano Compound Delta is composed of a coastal coarse-grained delta of reduced thickness and a muddy subaqueous clinoform up to 30 m thick.

In the Manfredonia Gulf, the Gargano subaqueous delta [35] deposited on the eastern and southeastern sides of the Gargano Promontory. This delta represents the southernmost portion of the Holocene highstand system tract (HST). The HST lies above a regional downlap surface (maximum flooding surface; mfs) that marks the time of the maximum landward shoreline shift (ca. 5.5 cal. ka BP) at the end of the last sea-level rise [14,30,35,36].

3. Methods

3.1. Seismic Surveys, Seismic Facies and Unconformity-Bounded Seismic Units

Seismic surveys were carried out in the Manfredonia Gulf (southern Adriatic) in 2016 and 2017 using the motorboat "ISSEL", owned by the Interuniversity Consortium for Sea Sciences (Con.I.S.Ma.). The following instruments and sensors were mobilised: (i) AppliedAcoustic Squid CSP-P 350J "sparker" source; and (ii) Geo-Resources Geo-Sense single-channel seismic acquisition system with 8 hydrophone streamers and amplification/filtering stages.

The seismic survey comprised 15 profiles oriented perpendicular to the coastline and 12 profiles subparallel to the coastline for a total of ca. 580 km (Figure 1). The minimum and maximum water depths were <8 m and ca. 97 m, respectively.

The data was processed using the IXSEA DELPH software. Through the use of the system, all the necessary steps for filtering, gaining and interpreting the data were performed.

Track-line positioning is based on D-GPS navigation, assuring a sub-metric position accuracy using the WGS84 datum.

The data were subsequently converted into a digital format/image for interpretation. Each seismic profile was imported into TEI Delph Map with Seismic GIS, allowing for immediate georeferencing and interpretation of acquired data. Finally, a buried erosional surface (ES1) was reconstructed using a triangular interpolation method in GIS.

For this work, seismic facies and Unconformity-Bounded Seismic Units (UBSUs) belonging to the transgressive system tract were identified.

The criterion used for the recognition and interpretation of seismic facies ([27]; Tables 1 and 2) is based on the individuation of groups of similar reflections based on form, continuity, amplitude, and frequency. We also used the spatial extension of seismic facies, along with the reciprocal position between facies, to infer depositional environments and formative processes. In addition, the literature interpretation on seismic facies was used to improve the seismic facies interpretation work (e.g., [13,30,31,36,39–43]). The seismic facies interpretations are also based on the data of two vibrocores drilled in 2015 in the Manfredonia Gulf (Figure 1): SP1_VC24 (intercepted by profile P2) and SP1_VC25 (close to profile PX2) on behalf of the Puglia Basin Authority (AdB). We did not directly observe these two vibrocores, but the corresponding data, provided by AdB, have been extensively described in De Santis et al. [27].

Table 2. Simplified sketch and short description of seismic facies 7, recognised within the UBSUs belonging to the TST in the Manfredonia Gulf area.

Seismic Facies	
7 	Description: irregular, strictly undulated reflectors of medium–low amplitude and medium-low lateral continuity. Alternatively, seaward–inclined reflectors, subparallel to the underlying ES1 or with a greater inclination. In some cases, this facies transitions seaward into facies 3
	Interpretation: slope deposits

Along with recognising the seismic facies, we identified the discontinuity surfaces, interpretable as surfaces of erosion or discontinuity in the sedimentation: they were used to separate the transgressive system tract sediments into UBSUs. In some cases, UBSUs are composed of a single seismic facies; in other cases, they are composed of multiple seismic facies that transit into one another (i.e., seismic units described in [7,44]).

3.2. Sea-Level Rise and Age Range Evaluation Method

For sea-level rise, we considered the local sea-level curve (site 25 in [45]), interpreted taking also into account Lambeck et al.'s curve [46] and Liu and Milliman's curve [47], in particular for the occurrence of MWP-1A and MWP-1B. In the curve of Lambeck et al. [45] both the MWP-1A and the following period of a much-reduced rate of rise corresponding to the timing of Younger Dryas are detectable. The following MWP-1B is less detectable but, in any case, also the local curve of Lambeck et al. [45] shows a relatively increased rate of rise after the Younger Dryas. Although the Liu and Milliman sea level curve [47] is contentious, in particular regarding the occurrence of MWP-1B (e.g., [46,48]), many regional studies [7,39], also in the Mediterranean ([6,13,49–51], among others), used that curve for the interpretation of the stratigraphic architecture of the transgressive units.

For an approximate assessment of the age range of the UBSUs, we used the method based on the current depth of the units correlated with the considered sea-level curve, assuming that the vertical movements of the substrate in the area are negligible compared with the eustatic component.

The method of age assessment based on the current position of the units has already been applied in the southern Adriatic (see, for example, the age estimation performed by [30] for units 2C and 2D of area 3 of the MIV or the age estimation of the Paleo Gargano Compound Delta performed by [38]). For the Manfredonia Gulf, this method has been chronologically constrained in De Santis et al. [27].

4. Data and Results

In this study, we present some of the results of the seismic survey carried out in the Manfredonia Gulf (southern Adriatic) in 2016 and 2017. In particular, the Ofanto valley and the transgressive architecture until the end of MWP-1B are described.

4.1. Ofanto Valley

In this work, the Ofanto incised valley is described for the first time in its entirety (Figure 2). In De Santis et al. [27], only the landward part of the valley extending up to the Barletta strait (called OSFV; Figure 1), along with the CCV (Figure 1), have already been described.

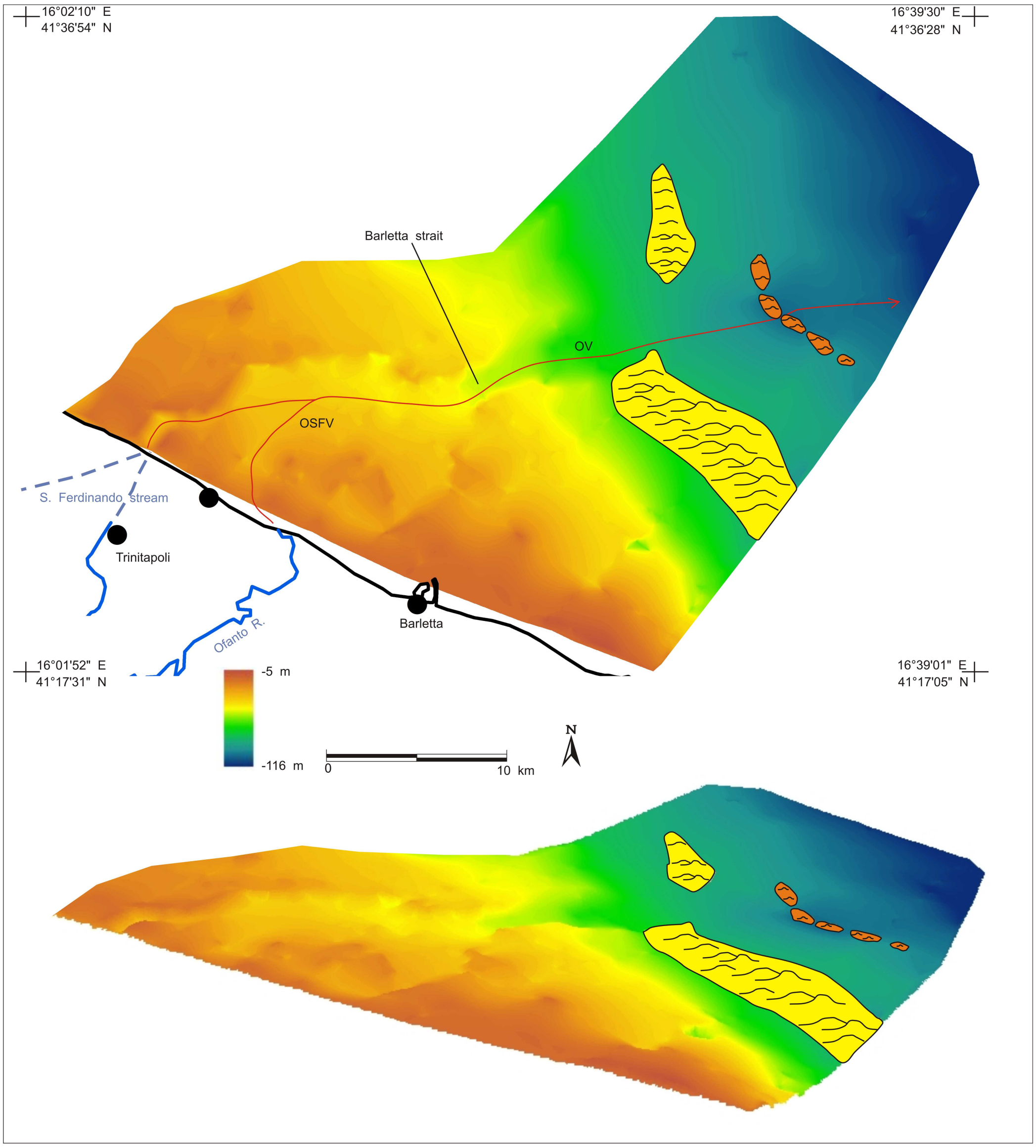

Figure 2. Digital Elevation Model (DEM) of the erosional surface (ES1) around the Ofanto valley both in plan view (**up**) and in oblique view (**down**). In orange and yellow with mounded morphologies drawn, the extension of facies 2 bodies into dune-like/barrier morphology of unit A_l and B_m, respectively.

Overall, the incision connected to the Ofanto River cuts the ES1 surface (Figure 2) and, on its landward side, it appears as two different subincisions. These subincisions merge in a single wide and shallow valley (OSFV). The OSFV reaches a maximum width of 11.9 km and narrows to ca. 2.5 km at the Barletta strait [27]. The OSFV reaches depths between ca. −15 m and ca. −50 m b.s.l. at the Barletta strait. With respect to the surrounding ES1, the valley shows decreasing depths toward the open sea, between ca. 17 m and less than 10 m. Outside the Barletta strait, the valley widens again without reaching the width of the OSFV, and since the incision is due only to the Ofanto River, we call this valley reach the Ofanto valley (hereinafter OV). The OV turns clearly toward the ENE; in this middle-distal sector, the valley reaches a maximum depth of ca. 14 m (profile T3, Figure 3) below the surrounding ES1, and a maximum width of ca. 8 km. The OV ends below the sedimentary lobe attributed to the Manfredonia incised valley [30]; this lobe, up to 15 m thick, lies just above the ES1. The lobe consists of ca. 0.6 km^3 of sediment, extending over an area of ca. 200 km^2 [30].

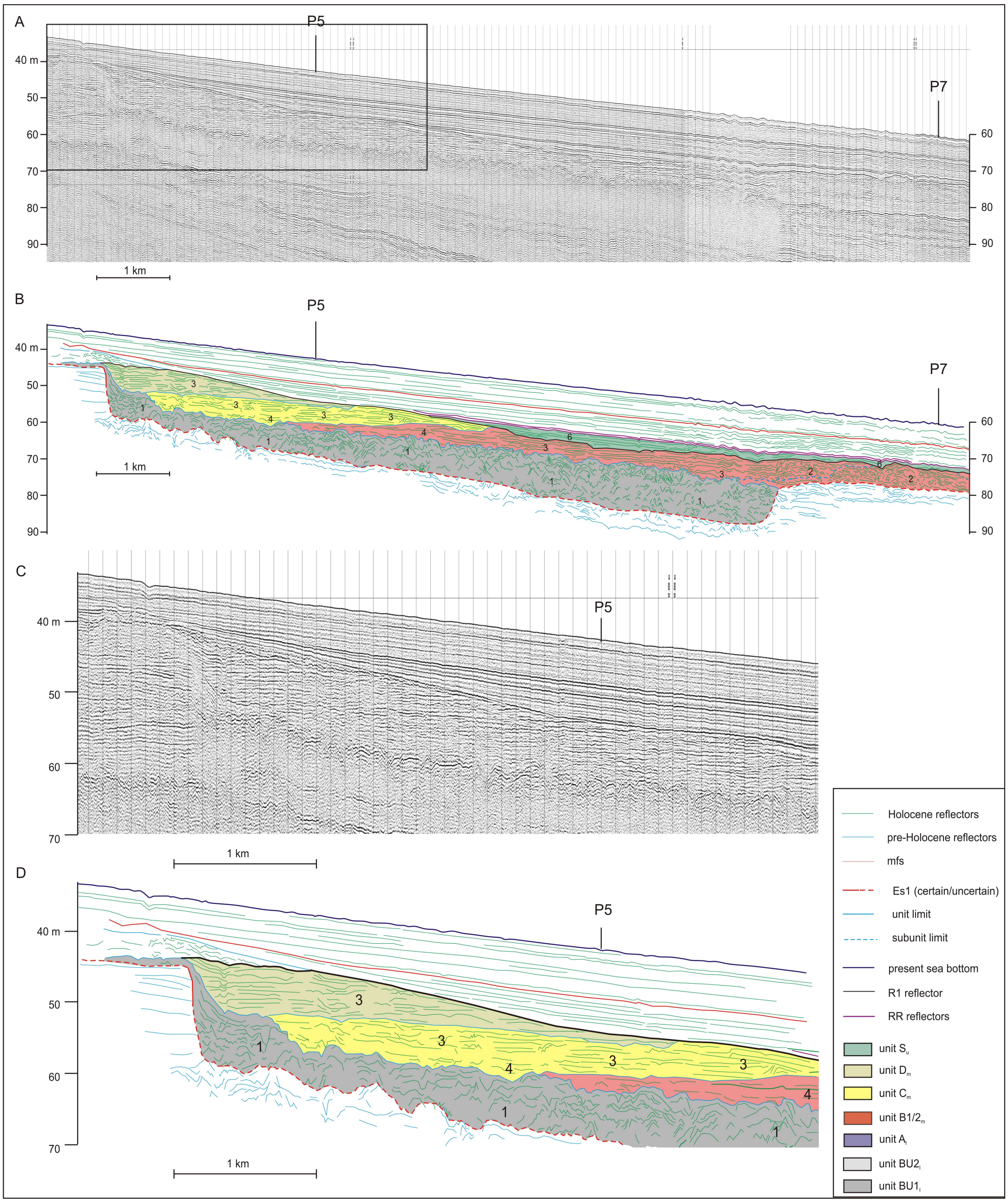

Figure 3. Part of seismic profile T3. Seismic section (**A**) and interpretation (**B**). (**C**,**D**) report an enlargement and its interpretation of the seismic profile sector included in the rectangle reported in (**A**). Note the Ofanto valley (OV) and the thick basal infilling by basal unit (BU)1_l, the coastal system of unit B_m, with subunits arranged in continuous landward backstepping pattern, and the stratal pattern of units C_m and D_m with reflectors of seismic facies 3 and 4 that onlap onto basal unit $BU1_l$ and are in turn truncated by surface R1. The legend reported in this figure applies for the following figures until Figure 10; the numbers reported in the interpretations of the figures indicate seismic facies; vertical scales are in metres below present sea level.

4.2. Transgressive System Tract

4.2.1. Seismic Facies

In this section, we summarise (Table 2) only the new seismic facies 7 recognised into the transgressive system tract. All other seismic facies have already been described and interpreted from a palaeo–environmental point of view in [27] (see Section 2 Regional Setting and Table 1).

4.2.2. Unconformity-Bounded Seismic Units

The seismic profiles highlight different UBSUs which we attributed to the lower, middle and upper transgressive system tract, based on their current depth, in accordance with Maselli and Trincardi [30] and Pellegrini et al. [38] for adjacent areas. The UBSUs are arranged in a landward backstepping pattern and cover ES1 and/or infill the Ofanto valley (OV). The subscript letters l, m, and u in the abbreviations of the UBSUs indicate their belonging to the lower, middle and upper transgressive system tracts, respectively. The unconformities that are characterised by high lateral continuity and high amplitude have been described and defined with an abbreviation.

The first units deposited above ES1 have been defined as basal units: basal unit 1 ($BU1_l$) and basal unit 2 ($BU2_l$), distinguished based on their different seismic facies and positions.

$BU1_l$ is present exclusively within the OV. In profiles P5, T2 and T3 (Figure 3), $BU1_l$ fills the OV, up to a maximum thickness of ca. 13 m. In profile T3, moreover, near the intersections with profile P5, the OV dextral slope is evident; $BU1_l$ rests both on the slope and on the bottom of the valley and consists of seismic facies 1.

$BU2_l$ extends from the seaward limit of the profiles to a minimum depth of ca. −90/−85 m b.s.l. (Figure 4). This unit mainly consists of two seismic facies. The deeper of the two is seismic facies 5, which reaches a considerable thickness, up to ca. 10 m, and has low amplitude, gentle seaward-downlapping reflectors topped by subhorizontal reflectors (profile T1; Figure 4); toward its basinward edge, seismic facies 5 shows a sigmoidal external shape. The second is seismic facies 2, characterised by a lack of organised reflectors, which appear somewhat chaotic (Figure 4). Seismic facies 2 appears superimposed and landward-displaced with respect to the underlying seismic facies 5.

Unit A_l is the most difficult to define due to the unconformities that bound it, which are not always clearly distinguishable. This unit is generally thin and is found at depths between a maximum of ca. −90/−85 m b.s.l. and a minimum of ca. −80/−75 m b.s.l. (Figure 5). When complete, unit A_l shows that, landward to seaward, seismic facies 3, 2 and 6 smoothly transition into one another. Within this unit, along a well-defined alignment (intercepted longitudinally by profile P7 and transversely by profile T1 and T2; Figures 2, 5 and 6), a sedimentary body, formed by seismic facies 2, is observed up to a maximum thickness of ca. 8 m, topped by a surface with a dune-like/barrier morphology, and characterised by high amplitude bidirectional downlapping reflectors. This body lies between −85/−80 m b.s.l.

The B_m unit is a complex system that, for most of its extension, lies directly above ES1 and, for minor parts, above A_l (Figure 7); it is found at depths between a maximum of ca. −80 m b.s.l. and a minimum of ca. −50 m b.s.l. The B_m unit is made up of two subunits, the oldest of which ($B1_m$) is located seaward; the younger ($B2_m$) is wider and appears retrograded and arranged in a continuous landward backstepping pattern (*sensu* [27]) with respect to the previous subunit (Figures 7 and 8). When complete, both $B1_m$ and $B2_m$ consist of the following seismic facies, which smooth transition into one another: from landward to seaward, seismic facies 3 and/or 4, seismic facies 2, and seismic facies 6. In profile T1 only, the $B2_m$ unit appears with a large sector constituted by seismic facies 7, approximately 2 km long, whose reflectors transition into plane-parallel reflectors of facies 3 (Figure 7). Seismic facies 6 has a thickness of ca. 1–2 m and gentle basinward-prograding reflectors. The sedimentary bodies formed by seismic facies 2 of this unit (Figure 7), together with the analogues of unit A_l (Figure 6), are the thickest and largest of all the bodies formed by seismic facies 2 in other UBSUs recognised in this work. In fact, bodies of seismic facies 2 within B_m are up to ca. 8 m thick and consist of chaotic reflectors; in places, the highest parts are in wavy packages and have a dune-like/barrier morphology (Figures 2 and 7); seismic facies 3 is up to ca. 6 m thick.

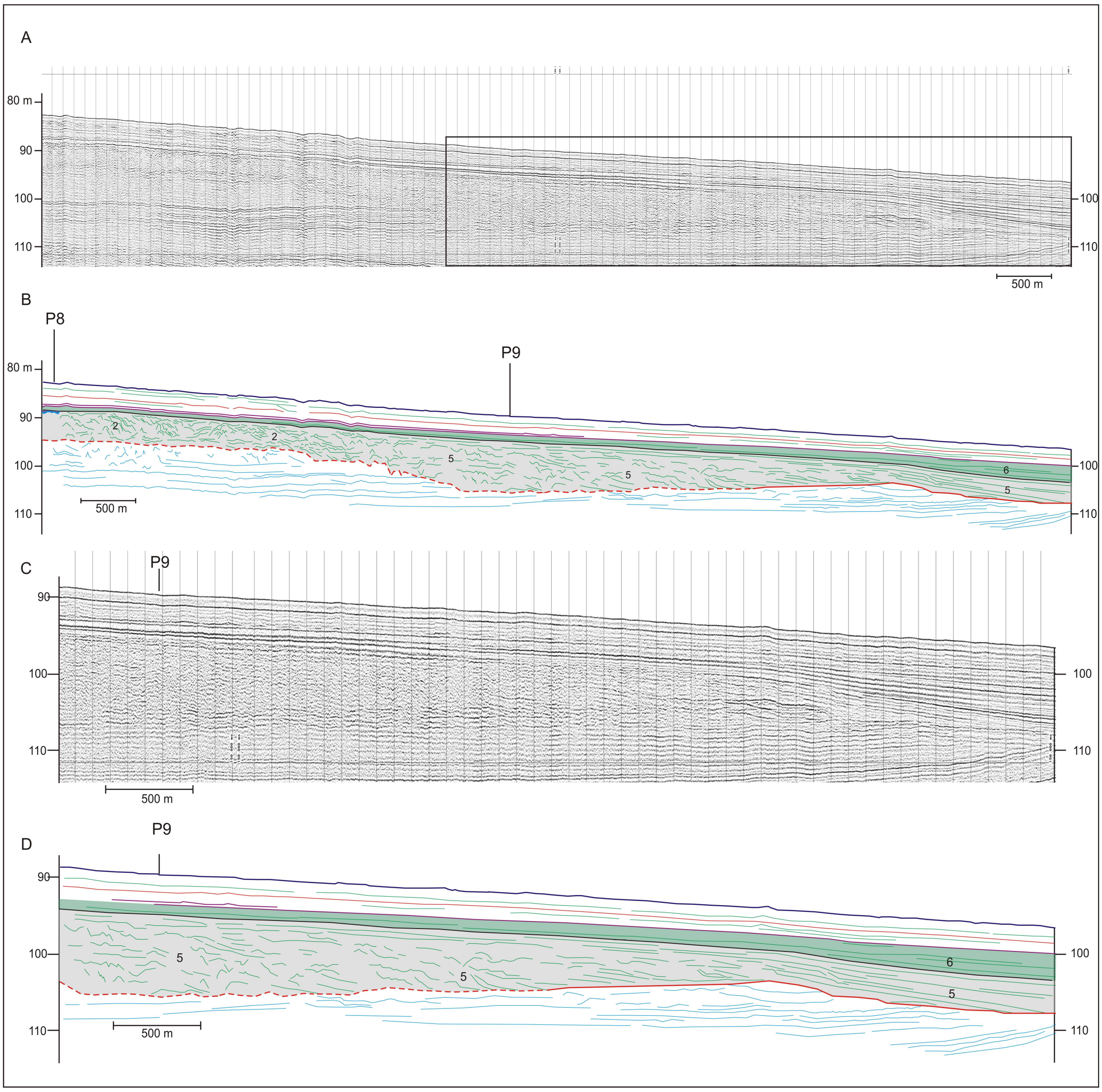

Figure 4. Part of seismic profile T1. Seismic section (**A**) and interpretation (**B**) showing, among others, unit $BU2_{l,}$ which occupies the deepest parts of the study area. (**C**,**D**) report an enlargement and its interpretation of the seismic profile sector included in the rectangle reported in (**A**). This unit seems compatible with the Manfredonia Incised Valley (MIV) depositional lobe, which we reinterpreted as a result of MIV and Ofanto deposition and thus renamed to the MIV and Ofanto depositional lobe (MOL): note the low-amplitude, gentle seaward-downlapping reflectors topped by subhorizontal reflectors.

In profile T2 (Figure 9), the $B1_m$ subunit consists of seismic facies 2, which passes landward/downward to a small body formed by seismic facies 3; the $B2_m$ subunit appears much more developed than the previous subunit and consists of seismic facies 2 in the central position, which changes seaward to reflectors in seismic facies 6 and landward, in the lower part of the unit, to reflectors in seismic facies 3. In profile P5, subunit $B2_m$ shows a change from seismic facies 2 outside the Ofanto valley to seismic facies 4 into the Ofanto valley, with evident channel features (Figure 10).

Landward along the ramp formed by ES1, other backstepped units are present: C_m and D_m, in which seismic facies 3 and 4 predominate with subhorizontal or slightly undulated reflectors (Figure 3). These units reach a maximum thickness of ca. 11 m in profile T3 (Figure 3).

The unit C_m is made up mostly of seismic facies 2 and 3. In profile T1, this unit, in the outermost part, exhibits a limited portion of chaotic reflectors in seismic facies 2 (Figure 7). In profile T2, C_m exhibits mostly seismic facies 2 (Figure 9). In profiles T3 and P5, this unit appears to be confined in the Ofanto valley and is made up of seismic facies 3 (Figures 8 and 10).

The unit D_m consists mainly of reflectors in seismic facies 3, with minor parts in seismic facies 2. In profile T1 (Figure 7), unit D_m exhibits seismic facies 2 overlying seismic facies 3. In profile T2 (Figure 9), unit D_m exhibits a small body in seismic facies 2, which transitions landward into seismic facies 3. In profile T3, unit D_m exhibits exclusively seismic facies 3.

All the units described so far are truncated at the top by a strong reflector (R1; Figures 3–9), which marks a clear discordance between the underlying subhorizontal reflectors of facies 3 or chaotic of facies 2 (belonging to units $BU2_l$, B_m, C_m, and D_m) and the other reflectors above, generally slightly seaward-inclined, ascribable to facies 6 and belonging to the subsequent unit S_u (Figures 3–9). In fact, the S_u unit is delimited at the bottom by the R1 reflector and at the top by a pair of strong reflectors with high amplitude and very high lateral continuity (RR reflectors; Figures 3–9); finally, the S_u reaches a maximum thickness of ca. 6 m.

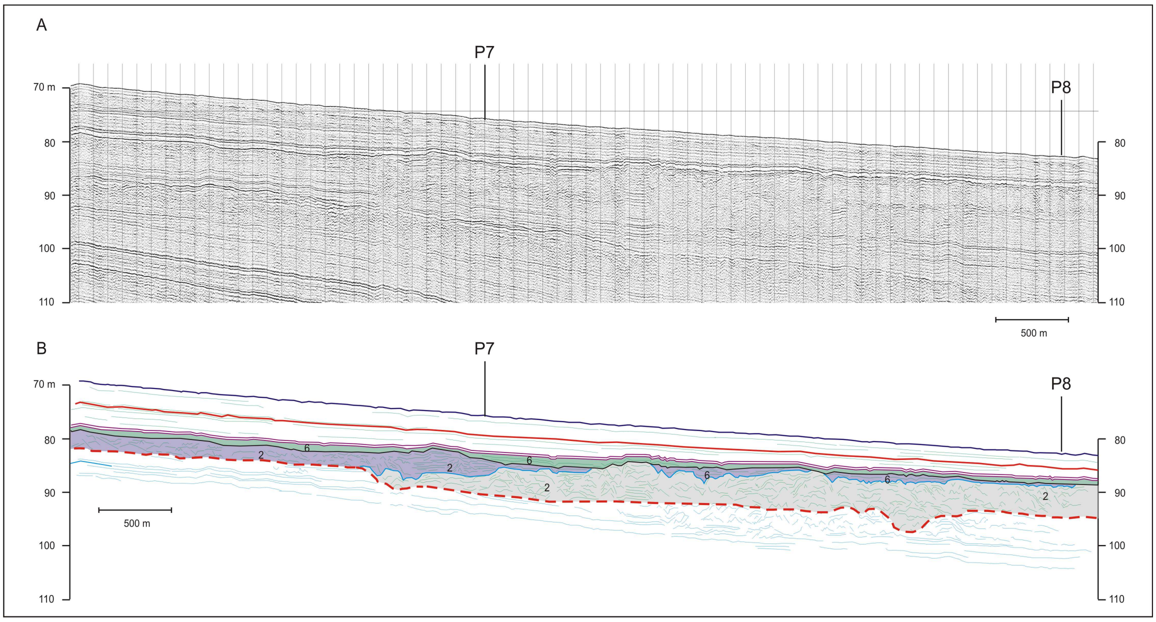

Figure 5. Part of seismic profile T1. Seismic section (**A**) and interpretation (**B**) showing, among others, unit A_l. Note the central part of the unit, made up of seismic facies 2 and modelled into a dune-like/barrier morphology.

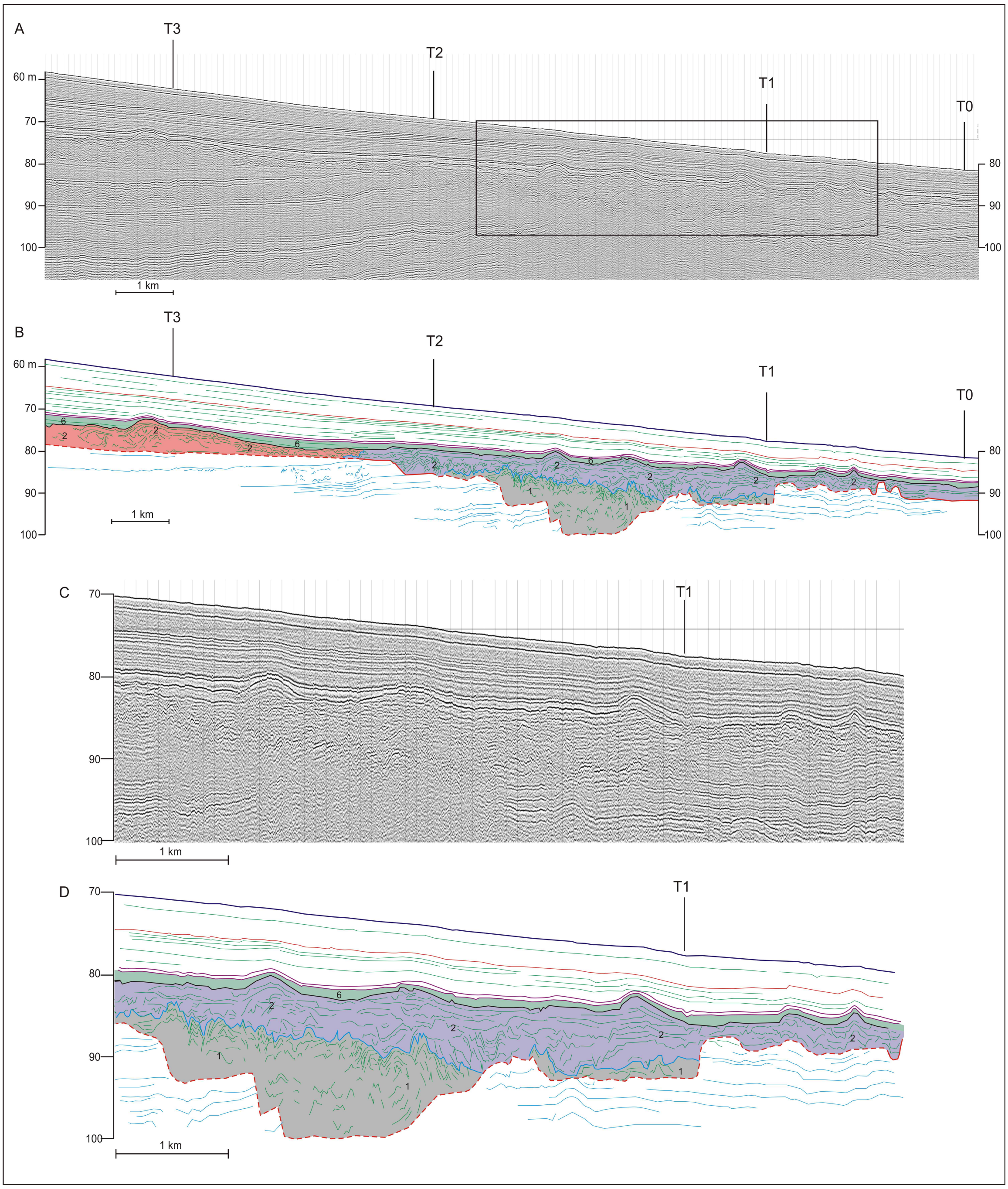

Figure 6. Part of seismic profile P7. Seismic section (**A**) and interpretation (**B**) showing, among others, the transversal section of the distal part of the Ofanto valley (OV), filled by unit $BU1_1$, and unit A_1. (**C**,**D**) report an enlargement and its interpretation of the seismic profile sector included in the rectangle reported in (**A**). Note, within unit A_1, the well-defined alignment, intercepted longitudinally by this profile, of the sedimentary body formed by seismic facies 2, topped by an irregular surface modelled into a dune-like/barrier morphology.

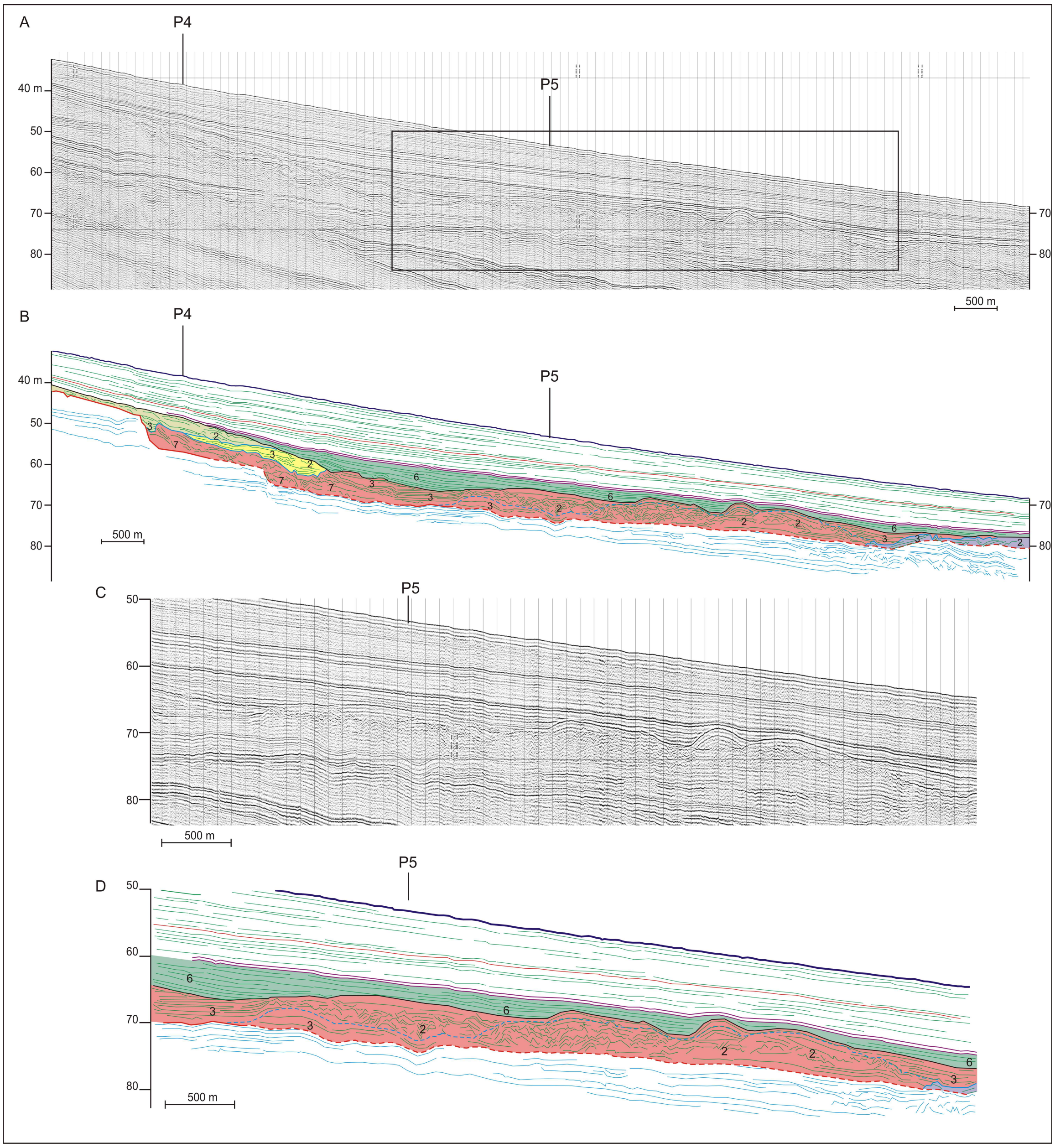

Figure 7. Part of seismic profile T1. Seismic section (**A**) and interpretation (**B**) showing, among others, units B_m, C_m, and D_m. (**C**,**D**) report an enlargement and its interpretation of the seismic profile sector included in the rectangle reported in (**A**). Note the dune-like/barrier morphologies within unit B_m; the older subunit ($B1_m$) is located seaward of the younger subunit ($B2_m$), which is wider and arranged in a continuous landward backstepping pattern (retrograded) with respect to the older one.

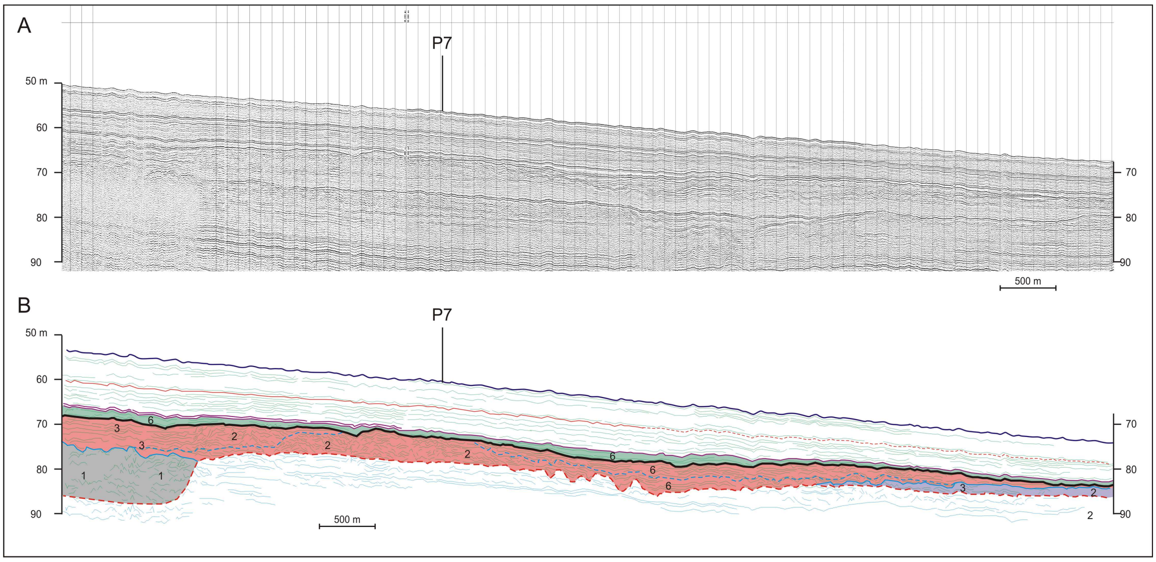

Figure 8. Part of seismic profile T3. Seismic section (**A**) and interpretation (**B**) showing, among others, units B_m with its subunits arranged in a continuous landward backstepping pattern.

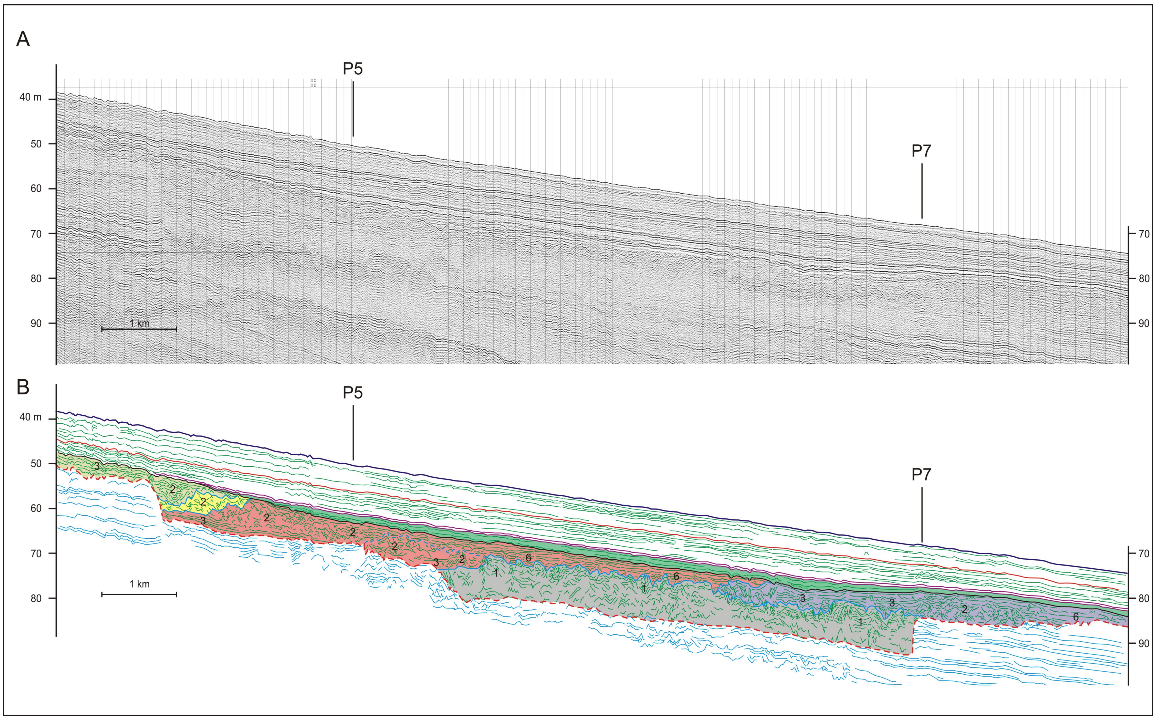

Figure 9. Part of seismic profile T2. Seismic section (**A**) and interpretation (**B**) showing, among others, the Ofanto valley (OV) with thick basal infilling by unit $BU1_l$ and units A_l, B_m, C_m, and D_m.

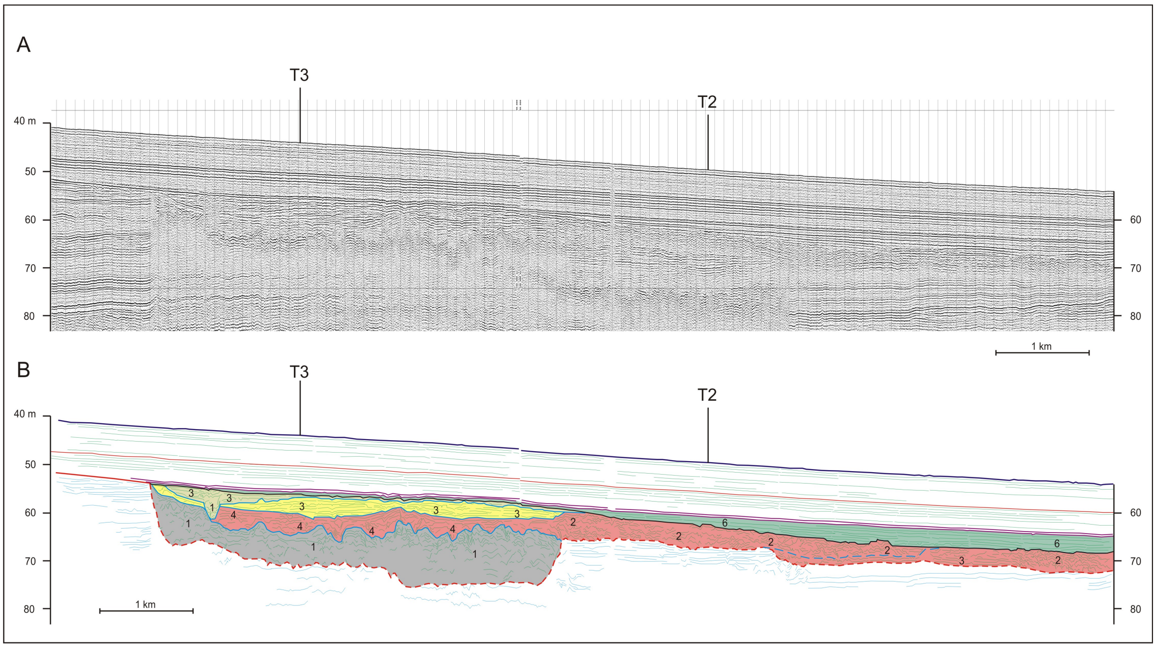

Figure 10. Part of seismic profile P5. Seismic section (**A**) and interpretation (**B**) showing the transversal profile of the Ofanto valley (OV) with thick basal infilling by unit BU1$_l$ and subunit B2$_m$, which shows a change of seismic facies 2 outside the OV to seismic facies 4 in the OV, with evident channel features.

5. Discussion

5.1. Ofanto Incised Valley and Its Differences from the Main Adjacent Incised Valleys

The catchments of the streams that cross the Tavoliere di Puglia Plain have been modified over time, including several captures [52,53]; in the coastal plain, the same streams changed their course and dispersed among the many coastal lakes that formed and evolved during the Holocene [54]. Therefore, the current catchments do not coincide with those during the last glacial maximum and the subsequent sea-level rise. For example, the San Ferdinando stream basin was part of the Ofanto basin, and the current Marana Castello basin was part of the Carapelle–Cervaro basin. The latter flowed into the Manfredonia incised valley (MIV) in the ES1 sector at the current water depth of ca. −25/−20 m.

The main feature of the Ofanto incised valley, considering both the stretch before the Barletta strait (Ofanto and San Ferdinando valley, OSFV) and the subsequent stretch (Ofanto valley, OV), is that it is a very wide and shallow valley (Figure 2).

The incision of the OSFV-OV dates to the last sea-level fall and last glacial maximum, with a sea level of ca. −134 m [46]. Its shape is very different from the nearby MIV, which is a deep erosional feature [32] with a depth below the ES1 and width decreasing seaward, changing from ca. 40 m by 7 km to ca. by 10 m by 0.3 km [30] (Figure 11).

A significant difference is also evident when comparing the OSFV-OV with the adjacent Carapelle and Cervaro valley (CCV) [27], which appears more similar in shape to the MIV than to the OSFV-OV (Figure 11). In fact, in the sector close to the modern coastline, this valley reaches a depth of ca. 30–37 m below the ES1 [27,32].

Such a difference could be explained by several causes. Many authors have summarised the main controlling factors that drive valley geometry; principal among these are the rate and magnitude of base-level fall [55,56], basin physiography [57,58], shelf-break depth [59,60], substrate type [61–64], tectonics [65–67], climate, and drainage-basin area [68–71].

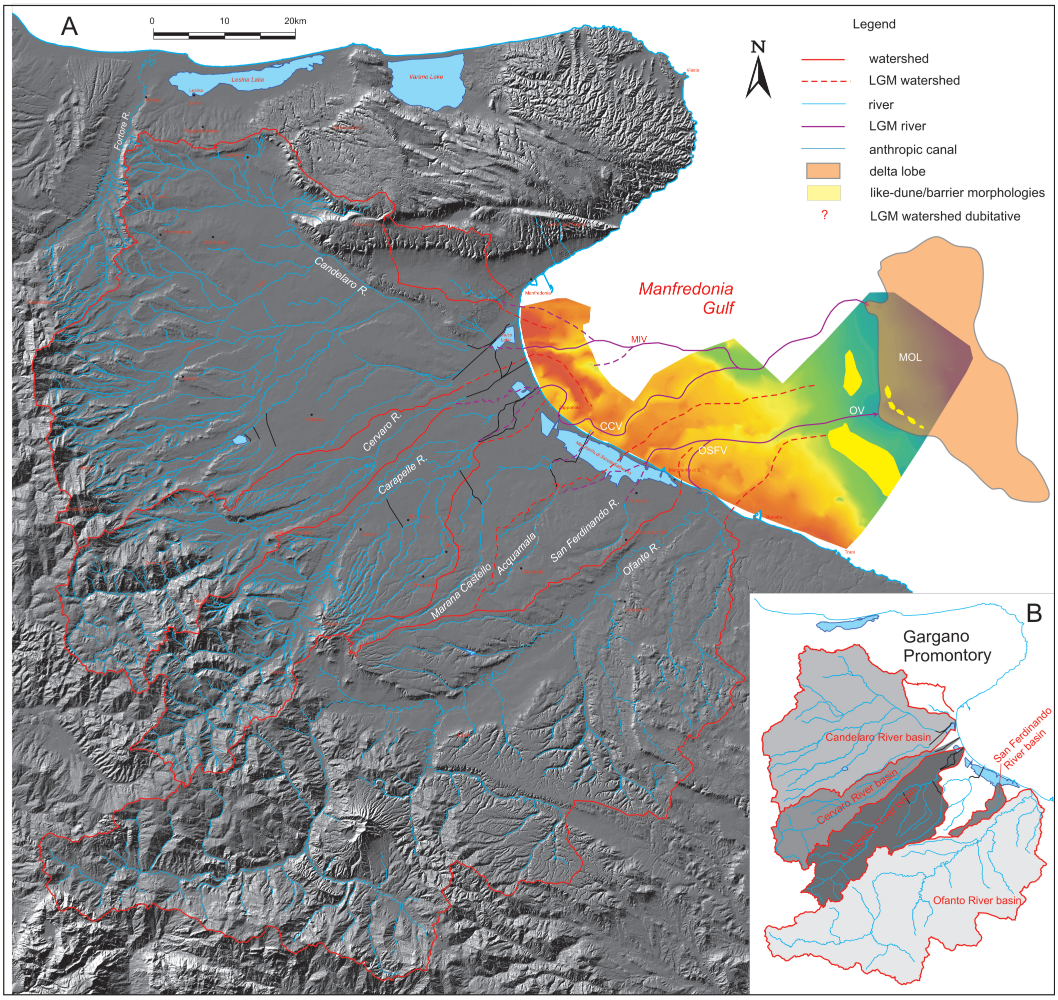

Figure 11. (**A**): Digital Elevation Model (DEM) of the study area and its surroundings. The inland DEM shows the present catchments of the main rivers draining the Tavoliere di Puglia Plain and the Gargano Promontory. The ES1 is shown offshore. On the ES1, the Manfredonia–Ofanto lobe (MOL) and the extension of facies 2 bodies modelled into the dune-like/barrier morphology of units A_l and B_m are shown. The reconstructed drainage network and watersheds are also shown along the ES1. (**B**): focus on the present catchments of the main rivers draining the Tavoliere di Puglia Plain.

Independent analysis of these main factors determining the shape of an incised valley shows that only one is significantly different among the MIV, CCV and OSFV-OV.

The rate and magnitude of base-level fall were not different between the three rivers because they flow into the southern Adriatic and are only a few kilometres apart.

The basin physiography, as well as the shelf-break depth and the substrate type, were almost identical between the three rivers. In fact, the lowstand subaerial shelf (ES1) shows an almost flat topography, plunging seaward with angles of ca. 0.03° and 0.09° [30]. Furthermore, the position of the lowstand shoreline for all rivers remains above the shelf edge; in fact, the sea-level fall of ca. −134 m at 20 ka [46] did not expose the entire shelf, since the shelf edge in the study area is at a water depth greater than 160 m [30]. Finally, MIV, CCV and OSFV-OV formed on previously deposited thick alluvial and marine sedimentary successions due to Quaternary cycles of sea-level oscillation [20,21,27,30].

Regarding the regional tectonics, the data available [19,27] do not highlight a significant difference in vertical movements between the different sectors of the coastal stretches of the Tavoliere di Puglia plain and Manfredonia Gulf and allow us to affirm that the whole area is characterised by negligible vertical movements during the Holocene.

However, the palaeo-climate could not have been significantly different during the incision phase, again due to the proximity between the three rivers.

Therefore, as the most likely factor to have determined the difference in shape between the three incised valleys, the difference between the drainage-basin areas remains (Figure 11). The Ofanto River, with a larger drainage area, gave rise to a wide and shallow valley. MIV and CCV, with a smaller drainage area, gave rise to narrower valleys, which were more deeply incised. This difference seems to respond to the dichotomy between conveyor belt vs. vacuum cleaner models for sediment supply, as it pertains to incised valleys and the dispersal of sediments to deepwater [68,72] (Figure 12). The conveyor belt model infers a large inland catchment, providing most of the sediments delivered to the shelf margin, whereas the vacuum cleaner model involves sediment production both from a small inland catchment and by excavating an incised valley. In other words, the increased erosion, due to the sea-level fall, was distributed among all the rivers or over a large area in the larger catchments, whereas in the catchments that were not large enough to provide the required sediment, cannibalism of the higher-order river occurred, inducing a stronger incision. Calculations demonstrate that the volume of sediments excavated from an incised valley is a small fraction of that delivered by the conveyor belt [68]. The difference in the thickness of the basal alluvial deposits in the filling of the OV (Figures 8 and 9) and MIV [29] seem to confirm that a conveyor belt model and a vacuum cleaner model are appropriate, respectively. In addition, a significant part of the drainage area of the MIV falls on the Gargano Promontory (Figure 11B), where Mesozoic limestones crop out [32]; thus, the sediments delivered by this part of the MIV catchment are negligible; this aspect contributed to a deeper incision of the MIV in response to the base level lowering.

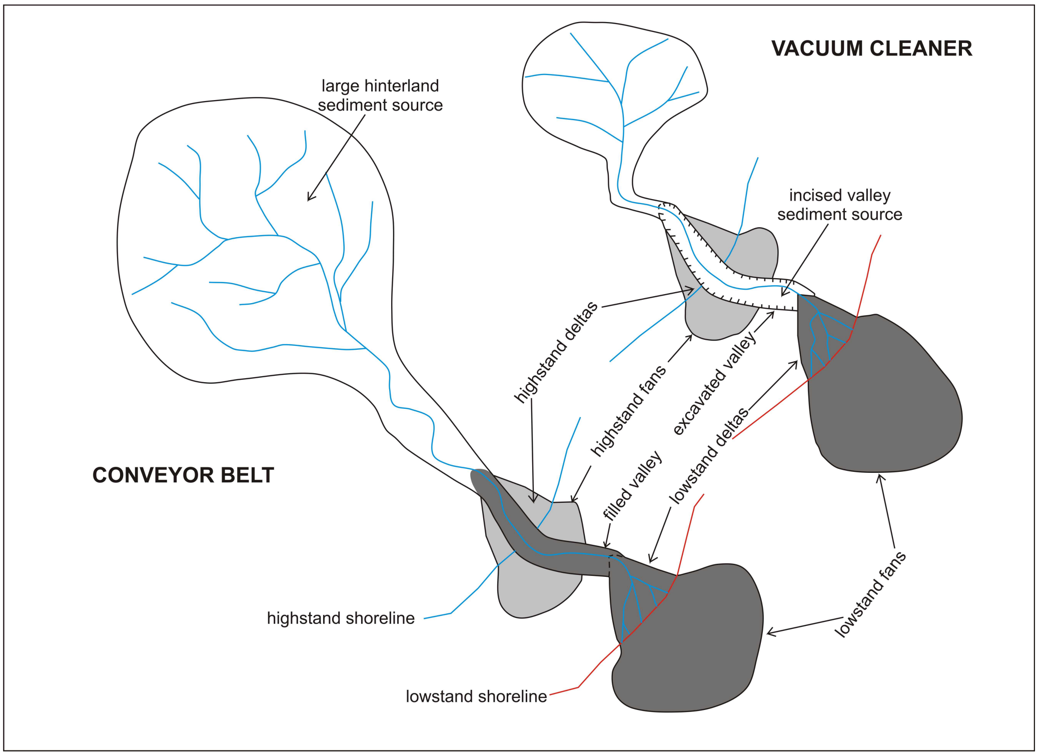

Figure 12. Vacuum cleaner vs. conveyor belt models for sediment supply for basin margins (modified from [68]). In the vacuum cleaner model, the sediments derive both from a deep valley incision and a small drainage area. In the conveyor belt model, sediments derive from a large hinterland catchment and a deep incision of the higher-order river is not required.

5.2. Transgressive System Tract

5.2.1. Unit $BU1_l$

Based on the evidence that $BU1_l$ lies within the OV (Figures 3, 6, 9 and 10) and is composed of seismic facies 1, we interpret this unit as an alluvial deposit. $BU1_l$ accumulated partly during the sea level drop phase, partly during the lowstand, and partly during the subsequent sea-level rise.

5.2.2. Unit $BU2_l$

$BU2_l$ occupies the deepest parts of the study area (Figure 4), until a current water depth of ca. −85 m b.s.l. The position of this unit, as well as seismic facies that constitute it, seem compatible with the MIV depositional lobe described by Maselli and Trincardi [30]. The presence of two seismic facies can be interpreted as subdivision of the delta into subenvironments with different energy conditions. Facies 5 is interpreted as the underwater part of the delta, while facies 2 is interpreted to be connected to the coastal part of the delta, deposited at or close to sea level. However, based on the identification of the OV, we can affirm that this depositional lobe derives from the fusion of two lobes: one of the MIV and one of the Ofanto (hereinafter called the MOL: the MIV and Ofanto depositional lobe) (Figure 11).

According to Maselli and Trincardi [30], the depositional lobe was likely deposited prior to MWP-1A which, in the study area, started ca. 14.4 cal. ka BP and ended ca. 13.5 ka cal. BP [45], with a local sea-level rise from ca. −93 to ca. −77 m b.s.l. [45]. Our data (current depth of unit $BU2_l$ and internal organisation and palaeoenvironmental interpretation of its seismic facies) confirm that the depositional lobe was deposited prior to MWP-1A (Figure 13A).

5.2.3. Unit A_l

Within this unit, the dune-like/barrier morphology at the top of the sedimentary body represented by seismic facies 2 (profile P7; Figures 2 and 6) has important significance. For both its characteristics, it can be interpreted as a residual of a coastal body (beach/shoreface/barrier (bsb) with dune-like morphologies) deposited at (or close to) sea level. Since this sedimentary body extends mainly in a modern water depth of ca. −85/−80 m b.s.l., we can approximate its age to ca. 13.9–13.7 ka cal. BP by correlating the body depth to the sea-level curve of Lambeck et al. [45]. Consequently, the unit can be ascribed to the MWP-1A.

The age attributed to unit A_l must be considered with other interpretations. The first is that unit A_l, with its dune-like belt (see profile P7, Figure 6), is the coastal part of the MOL, which would thus be interpretable as a compound delta, where a coastal sandy deposit is genetically linked to distal subaqueous progradation (unit $BU2_l$). The morphologic profiles of compound systems are characterised by a couple of rollover points (i.e., coastal and subaqueous rollover points [73]), and this is what is observed in the case of the nearby Palaeo Gargano Compound delta (PGCD), formed offshore of the modern Gargano Promontory within the middle TST [38]. In the PGCD, the coastal coarse-grained deposit formed at the shoreline with a coastal rollover point at a palaeo-water depth of 3 m, while fine-grained sediments accumulated in deeper shelf environments with a subaqueous rollover point at a palaeo-water depth of 28 m, with a difference in water depth of ca. 25 m between the coeval coastal and subaqueous rollover points, similar to the distance found in the modern Adriatic compound delta (ca. 25–30 m; [37,74]).

Since the subaqueous rollover point of the MOL in the sector we investigated is ca. −97 m b.s.l. (profile T1, Figure 4), the dune-like belt of unit A_l, between −85 and −80 m b.s.l. (that is, with a difference in water depth of ca. 12–17 m) could represent the coastal coarse-grained deposits of the MOL, although without an evident coastal rollover point. In this case, however, the MOL would not be like the nearby and contemporary PGCD but rather to the modern Po River delta, where the subaqueous lobe formed at water depths between 2 m and 10 m [30,75].

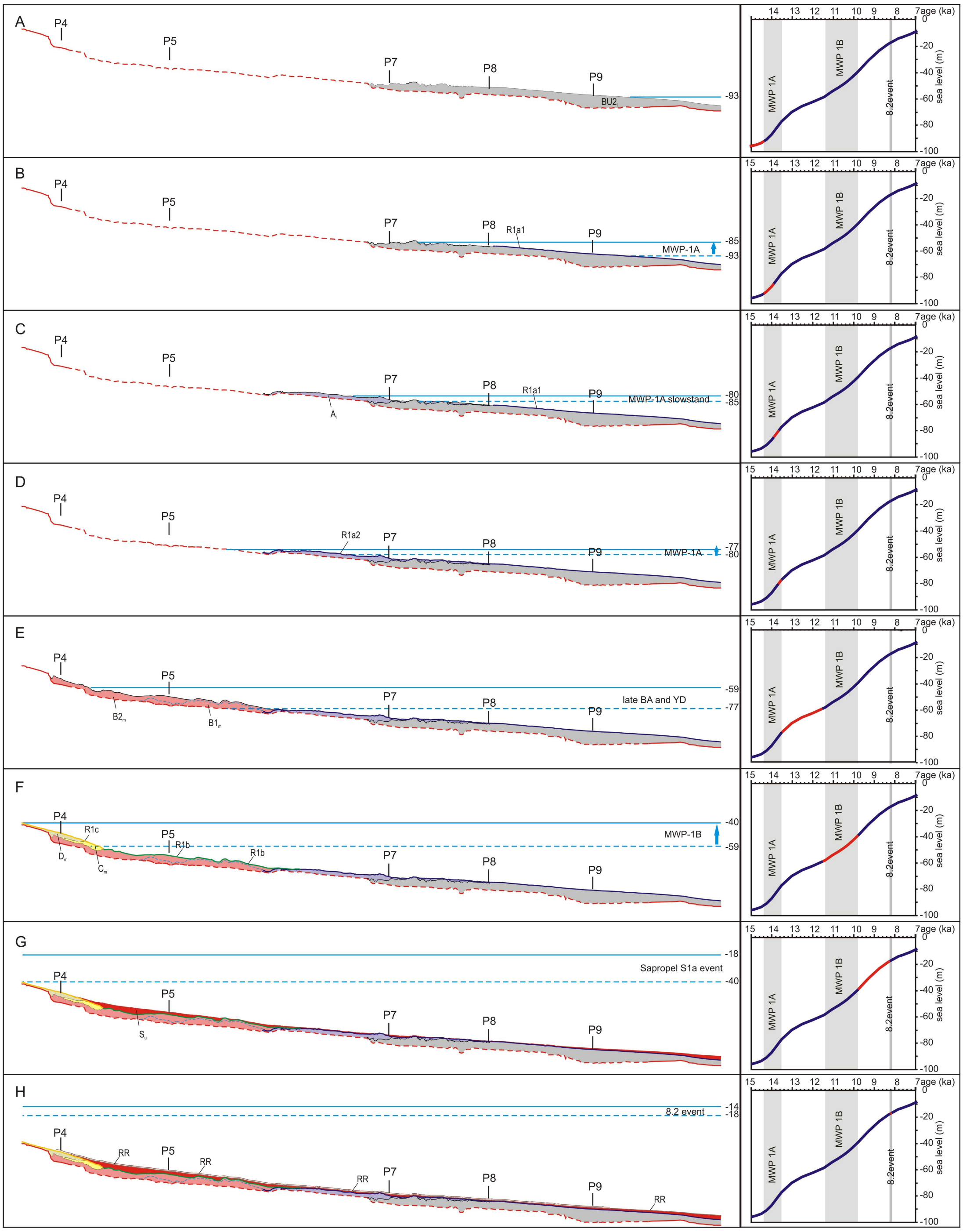

Figure 13. Phases of deposition of the UBSUs reported in profile T1 and plotted on the sea level curve by [45] (right side). For the description of the steps (**A**–**H**), see the text. BA = Bølling Allerød; YD = Younger Dryas.

However, following the hypothesis that unit A_l is the coastal part of the MOL, this would imply that the MOL would have formed when the sea level was between −85 and −80 m b.s.l., and therefore during MWP-1A (Figure 14). Thus, unit A_l should be incorporated into unit $BU2_l$. This interpretation conflicts with the evidence that MWP-1A inhibited the formation of deposits of significant thickness in the Adriatic; indeed, the two meltwater pulses caused short-term decreases in sediment flux likely related to major changes in the river equilibrium profile forced by rapid sea-level rise, causing the bedload to be trapped in alluvial plains through channel aggradation and flood plain construction [13,37].

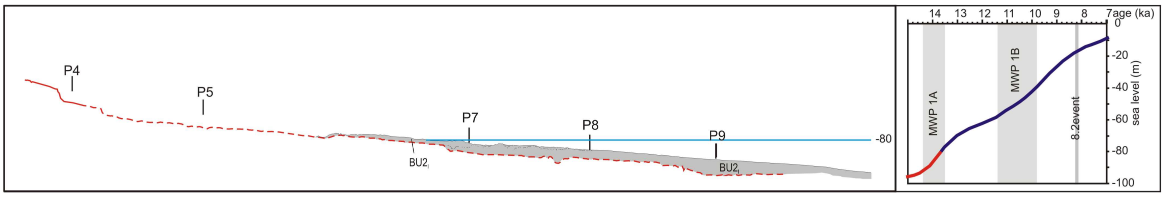

Figure 14. Alternative interpretation of unit A_l considered the coastal part of the MIV and Ofanto depositional lobe (MOL).

The alternative interpretation would be that unit A_l is a second small depositional lobe deposited at (or close to) sea level due to the Ofanto sediment discharge, arranged in a landward backstepping pattern with respect to the greater MOL (Figure 13B,C). This situation is similar to that of the Thukela Shelf (South Africa), where two prograding and backstepped sandy delta systems at depths of 40 m and 32 m have been recognised [76]. Delta development was favoured during sea-level stillstands at −40 m and −32 m, respectively, while the step-back of the deltas corresponded to sharp increases in the rate of sea-level rise associated with meltwater pulses.

In our case, the small depositional lobe of Ofanto represented by unit A_l and backstepped with respect to the larger MOL could have formed due to a slowstand (sensu [7,8] among others) during MWP-1A (Figure 13B,C) and then overstepped in the remainder of MWP-1A (Figure 13D). Considering the age attributed to unit A_l of ca. 13.9–13.7 cal. ka BP [45], this slowstand may have been caused by the contemporary end of the first warm peak of the Bølling-Allerød [77].

Further studies will be needed to definitively clarify whether unit A_l, with its dune-like features, represents the coastal part of the MOL or another small depositional lobe backstepped with respect to the greater MOL and dating back to a very short (centennial scale) slowstand during the MWP-1A. Although the centennial scale of unit A_l is a very risky interpretation, we favour this hypothesis, which corresponds to the interpretations of our seismic profiles.

5.2.4. Unit B_m

We interpret unit B_m as a complex coastal system consisting of residual of backbarrier, barrier (with dune belts, beach, foreshore, and shoreface) and offshore deposits. This system comprises two subsystems. The first, represented by the $B1_m$ subunit, consisting of a central body interpreted as a bsb deposit topped by subparallel dune-like morphologies and intervening depressions (Figures 2 and 7). This central body transitions seaward to a lower shoreface/offshore and landward to a slightly extended backbarrier. The second, wider subsystem, represented by subunit $B2_m$, appears arranged in a continuous landward backstepping pattern [27] with respect to $B1_m$, with an evident organisation in subenvironments that, from seaward to landward, transitions from offshore/lower shoreface to bsb (Figures 2, 7 and 9) to backbarrier and, in the case of profile T1 (Figure 7), even to slope deposits that fall into the backbarrier deposits.

Given that the coastal part of B_m (dune-like morphologies and bsb deposits formed by seismic facies 2, and backbarrier formed by seismic facies 3 or 4) is at a modern water depth of ca. −75/−60 m, we conclude that the unit was formed due to the slowstand that occurred after MWP-1A. On the whole, this slowstand led the sea to rise, in the study area, from ca. −77 to ca. −59 m b.s.l.; this phase started ca. 13.5 cal. ka BP and underwent a further deceleration from ca. 13 cal. ka BP [45] to ca. 11.4 cal. ka BP [45,73]. This slowstand is coeval to the late Bølling Allerød and the Younger Dryas (Figure 13E), and it was probably accompanied by an increase in the sediment supply to the sea. Changes in precipitation rates and vegetation cover related to the Younger Dryas event may have resulted in higher sediment production in the catchments and higher rates of sediment input to the sea that favoured the formation of progradational deposits [15,78]. This enhanced sediment input, along with the low-gradient setting and slow relative sea-level rise, promoted the continuous landward backstepping pattern that characterises the B_m subunits (Figure 15). This allowed the partial protection and preservation of the previous barrier system (subunit $B1_m$) from wave ravinement action due to the partial burial by subsequent subunit $B2_m$.

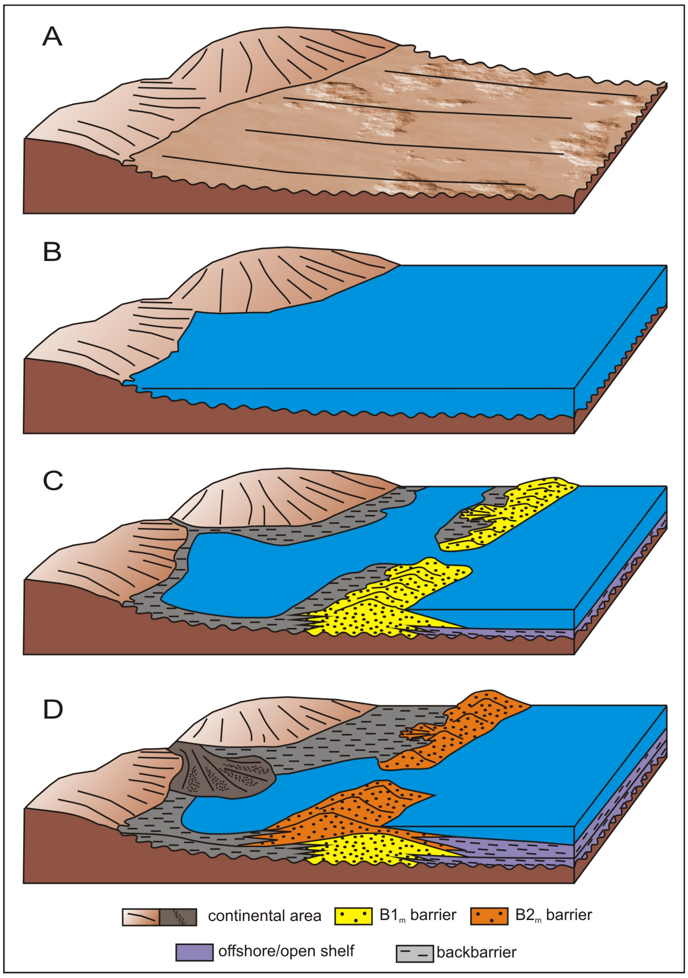

Figure 15. Evolution of unit B_m, with subunit $B2_m$ (orange) arranged in a continuous landward backstepping pattern with respect to subunit $B1_m$ (yellow). (**A**): emergence of the ES1; (**B**): drowning of the ES1; (**C**): slowstand and formation of the first subunit $B1_m$; (**D**): slowstand and formation of the second subunit $B2_m$, in a continuous landward backstepping pattern with respect $B1_m$.

Putting together the results of this work and those of De Santis et al. [27], it turns out that there were two distinct phases in which beach/barrier–backbarrier systems arranged in a continuous landward backstepping pattern were formed: a first during the Younger Dryas and a second coeval to the sapropel S1event (Figure 16). This is due to the fact that all three factors that favour this retrogradation pattern (enhanced sediment input, low-gradient setting and slow relative sea-level rise [27]) occurred together in these two periods. During the sapropel S1 event, the beach/barrier–backbarrier systems formed in a sector of the Ofanto valley more landward (OSFV) than that where unit B_m formed [27].

Starting from ca. 11.4 cal. ka BP, the age at which the Younger Dryas ends, a relatively increased rate of rise occurred in the study area, with a sea-level rise from ca. −59 to ca. −40 m, between ca. 11.4 cal. ka and ca. 9.8 cal. ka [45]; we identify this phase as the local expression of the MWP-1B [47], also on the basis of other evidences of this pulse in many areas of the Mediterranean continental shelves [6,13,49–51]. This phase of sea level rise caused the drowning and overstepping of unit B_m (Figure 13F). Thanks to this drowning, even the morphologies in the $B2_m$ subunit were partially protected from the wave ravinement action, so their morphologies were partially preserved.

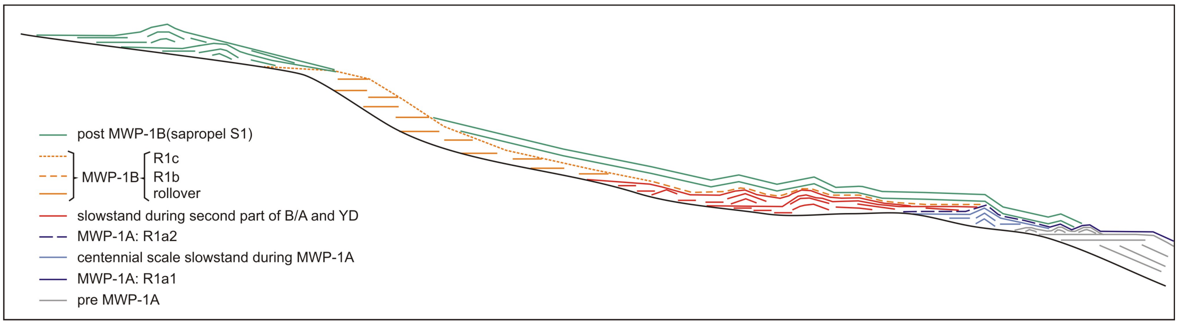

Figure 16. General model of transgressive architecture and stratal pattern of transgressive deposits recognised in the study area. Each colour corresponds to a phase of the transgression.

5.2.5. Units C_m and D_m

Units C_m and D_m lie in a current water depth between ca −60 and ca −40 m b.s.l. In addition, in their case, given this water depth range, it can be inferred that C_m and D_m formed during the sea-level rise that can be correlated to MWP-1B, that is, between ca. 11.4 and ca. 9.8 cal. ka [45] (Figure 13F). Their position with respect to unit B_m can be interpreted as an overstepping of the B_m unit; barrier overstepping has been attributed to a combination of rapid sea-level rises, such as those associated with meltwater pulses [79] or other particularly favourable circumstances, such as early cementation (beachrock and aeolianite formation) or gravelly sediments [2].

In our case, we have no elements to determine whether, in addition to the relatively rapid sea-level rise due to MWP-1B, other factors helped to trigger overstepping.

We believe that units C_m and D_m were originally made up of bsb and backbarrier, but that later wave ravinement almost totally destroyed the bsb part leaving only the backbarrier deposits. This process originated the stratal pattern of units C_m and D_m (profile T3; Figure 3), with reflectors of seismic facies 3 that onlap onto ES1 and/or $BU1_l$ and are in turn truncated by surface R1. As the sea-level rise proceeded, the coastal system formed by the bsb and backbarrier migrated landward by means of the continuous construction of a new system and the simultaneous partial or total destruction of the previous system by wave ravinement. This process partially protected the backbarrier deposits from wave ravinement due to their lower elevation and partial burial by a new barrier that formed more landward. This process is identifiable with the rollover which, unlike overstepping, does not leave relict barriers [2].

According to what we have reconstructed, unit B_m was preserved due to a drowning associated with MWP 1B and consequent overstepping; subsequently, there was a rollover of the coastal system. In profile T3, in particular, which intercepts the OV, the preserved backbarrier deposits dating back to the rollover migration of the barrier (units C_m and D_m) reach the greatest thicknesses, probably due to the higher sediment influx during transgression.

5.2.6. Reflector R1

The reflector R1 that delimits at the top all the transgressive units described so far, except for $BU1_l$, can be divided, from a genetic point of view, into three parts: (i) that corresponding to the top of units $BU2_l$ and A_l (R1a), which in turn can be divided into two subparts, R1a1 and R1a2; (ii) that corresponding to the top of the coastal-linked part of unit B_m (R1b); and (iii) that corresponding to the top of units C_m and D_m (R1c). These three parts can be interpreted as follows: (i) an erosion/non-deposition surface due to a drop in sediment delivery during MWP-1A; in particular, R1a1 formed in the first part of MWP-1A before the very short slowstand that gave rise to the formation of unit A_l (Figure 13B), whereas R1a2 formed during the second part of MWP-1A after the formation of unit A_l (Figure 13D); (ii) an erosion/non-deposition surface due to a drop in sediment delivery during MWP-1B (Figure 13F); and (iii) a wave ravinement surface (Figure 13F).

5.2.7. Unit S_u and Reflectors RR

The unit S_u is interpreted as transgressive marine mud. Since this unit lies above both unit B_m (referable to the late Bølling Allerød and the Younger Dryas) and units C_m and D_m (referable to the local MWP-1B), it is evident that unit S_u is younger than local MWP-1B. Consequently, it is highly probable that the unit S_u is contemporaneous with the sapropel S1 event (Figure 13G). In fact, more or less at the end of the local MWP-1B, occurred at ca. 9.8cal. ka BP with a sea level of ca. −40 m b.s.l. [45], the sapropel S1 event started; this event consists of the accumulation and preservation of organic matter in deep marine sediments due to increased precipitation and river runoff in northern Africa and the eastern European region, which led to water column stratification and reduced deep-water oxygenation. The sapropel S1 event occurred from ca. 10 to ca. 6.8 cal. ka BP [80,81], with a local sea-level rise from ca. −42 m b.s.l. to ca. −8 m b.s.l. [45], and formed in two distinct phases (S1a and S1b), which are separated by an interruption dating to ca. 8.3–7.8 cal. ka BP in the Adriatic Sea [81], with a corresponding sea level at ca. −18/−14 m b.s.l. [45]. This interruption is due to the so-called 8.2 event [82,83]: a short-lived episode of cooler and drier conditions [80], with an abrupt sea-level rise and an interruption in the sediment discharge in the Mediterranean.

Since the role of the sapropel S1a event in the Manfredonia Gulf in promoting the creation of extensive coastal barrier/backbarrier systems within the upper TST has already been demonstrated (units D_u, E_u, and G_u in De Santis et al. [27]), we believe that the unit S_u is the offshore counterpart of those coastal systems and is coeval with sapropel S1a.

Upward, the unit S_u is delimited by the pair of reflectors RR, which we interpret as the result of a sediment drop, perhaps a trace of the 8.2 event, which interrupted the formation of Sapropel S1 and therefore the discharge of a significant amount of sediment to the sea (Figure 13H).

5.2.8. Dune-Like Fields within Units A_l and B_m

The dune-like fields present within units A_l and B_m reflect the “in-place drowning” transgressive model for low-gradient shelves [84,85]: a barrier lagoon system developed during a slowstand; the barriers were drowned and preserved due to a rapid relative sea-level rise, such as the MWP-1A and MWP-1B. Later, a new barrier formed landward during a subsequent slowstand. This is the case, for example, in the barrier systems of the northern Adriatic [6], a low-gradient setting [37] where barrier overstepping and drowning occurred. As a result, two barriers can be preserved several kilometres apart. A similar case is that described in Tijucas Bay (southern Brazil) [39], where a former sandy shoreface barrier was overstepped during the 8.2 ka event and a new barrier formed at the landward margin of the former backbarrier (over a 7 km cross-shore distance).

A process similar to that which affected the barrier within unit B_m (and probably also the barrier within unit A_l, assuming that it represents a coastal barrier following the formation of the MOL) has been observed in the continental shelf off Durban, South Africa, where the presence of a remarkably well-preserved barrier complex has been documented [7,86].

The process that led to the formation and conservation of the barrier complex described by Green et al. [7] is similar to that of the barrier within the unit A_l only in terms of the type of process, while the similarity with the barrier within unit B_m concerns both the type of process and the time interval in which it took place. The same authors recognised the barrier complex at water depths between 50 m and 65 m: sea-level stability at the outer barrier position (ca. −65 m) enabled the accumulation of a coastal barrier that remained intact during a phase of subsequent slow sea-level rise to −58 m when the lagoon formed. Then, an abrupt rise in sea-level to −40 m, correlated with MWP-1B, enabled the preservation of the sea bed of the cemented core of the barriers described; in this case, early cementation played an important role in enhancing the probability of not only barrier overstepping but also preservation of the overstepped barrier.

In our case, we do not know if the dune barriers inside units A_l and B_m have undergone early cementation. Certainly, this is less likely, at least for the barrier present within A_l, due to the short time interval estimated for its formation, that is, from ca. 13.9 to ca. 13.7 cal. ka BP, while it is more probable for the barrier within unit B_m, which formed during a more prolonged period of relative shoreline stability.

Prolonged sea-level stability is considered as a major contributor to aeolian sediments having longer residence times in the vadose zone, thus favouring the rapid lithification of dune bases [77,78]. During the Younger Dryas, the associated slowstand allowed enough time for the construction and lithification of shoreline complexes, such as, probably, that within unit B_m.

6. Conclusions

The data collected in the Manfredonia Gulf and presented in this article, together with those already presented in De Santis et al. [27], allow us to outline a complete and more general model of the Holocene transgressive architecture in the Manfredonia Gulf of the southern Adriatic Sea.

This framework consists of the following phases, each of which involved a particular stratal architecture in the transgressive deposits (Figure 16):

- pre meltwater pulse 1A: construction of the Manfredonia–Ofanto Lobe;
- first part of meltwater pulse 1A: interruption of the sedimentation of the Manfredonia–Ofanto Lobe and formation of reflector R1a1;
- brief slowstand, perhaps at a centennial scale, during meltwater pulse 1A: construction of the coastal system of the A_l unit;
- the second part of the meltwater pulse 1A: drowning and overstepping of unit A_l; interruption of the sedimentation and formation of the reflector R1a2 on the unit A_l;
- slowstand during the late Bølling-Allerød and during the Younger Dyas: formation of the coastal barrier system of the B_m unit with a continuous landward backstepping process, due to the combination of the enhanced sediment input, low-gradient setting and slow sea-level rise;
- Meltwater pulse 1B: drowning and overstepping of the coastal system of the B_m unit and formation of the R1b surface. Simultaneously, rollover of the coastal system and formation of the R1c surface (wave ravinement surface);
- post Meltwater pulse 1B and Sapropel S1: renewal of the conditions for the construction of coastal barrier systems in a continuous landward backstepping pattern; in this case, the condition of enhanced sediment input was due to the Sapropel S1 event [27].

Author Contributions: Conceptualization, V.D.S., M.C., L.P.; methodology, V.D.S.; software, V.D.S., M.C.; formal analysis, V.D.S., M.C.; investigation, V.D.S., M.C.; data curation, V.D.S., M.C.; writing—original draft preparation, V.D.S.; writing—review and editing, V.D.S., M.C.; supervision, V.D.S., M.C., L.P.; funding acquisition, V.D.S., L.P. All authors have read and agreed to the published version of the manuscript.

Funding: This research received no external funding.

Acknowledgments: We are very grateful to (1) Puglia Basin Authority (AdB) for stratigraphic descriptions of vibrocores SP1_VC24 and SP1_VC25, obtained within the "*Piano operativo per l'individuazione di giacimenti di sabbia sottomarini utilizzabili per il ripascimento artificiale dei litorali sabbiosi in erosione della regione. P.O.R. Puglia 2000–2006-FESR-Asse IV sistemi locali di sviluppo, misura 4.16*"; (2) Con.I.S.Ma. (Interuniversity Consortium for Sea Sciences) for use of the motorboat "ISSEL", within the research agreement n. 270-2017 "*Rilievi sismici sulla piattaforma continentale pugliese*"; (3) Ionic University section of the University of Bari for instruments and sensors used for navigation and seismic campaign; (4) En.Su (Environmental Survey) and Francesco De Giosa for data processing.

Conflicts of Interest: The authors declare no conflict of interest.

References

1. Mellett, C.L.; Plater, A.J. Drowned Barriers as Archives of Coastal-Response to Sea-Level Rise. In *Barrier Dynamics and Response to Changing Climate*; Moore, L.J., Murray, A.B., Eds.; Springer: Cham, Switzerland, 2018; pp. 57–89. ISBN 978-3-319-68086-6.
2. De Falco, G.; Antonioli, F.; Fontolan, G.; Lo Presti, V.; Simeone, S.; Tonielli, R. Early cementation and accommodation space dictate the evolution of an overstepping barrier system during the Holocene. *Mar. Geol.* **2015**, *369*, 52–66. [CrossRef]

3. Green, A.N.; Cooper, J.A.G.; Salzman, L. The role of shelf morphology and antecedent setting in the preservation of palaeo-shoreline (beachrock and aeolianite) sequences: The SE African shelf. *Geo-Mar. Lett.* **2018**, *38*, 5–18. [CrossRef]
4. Pretorius, L.; Green, A.N.; Cooper, J.A. Submerged beachrock preservation in the context of wave ravinement. *Geo-Mar. Lett.* **2018**, *38*, 19–32. [CrossRef]
5. Zecchin, M.; Catuneanu, O.; Caffau, M. Wave-ravinement surfaces: Classification and key characteristics. *Earth-Sci. Rev.* **2019**, *188*, 210–239. [CrossRef]
6. Storms, J.E.A.; Weltje, G.J.; Terra, G.J.; Cattaneo, A.; Trincardi, F. Coastal dynamics under conditions of rapid sea-level rise: Late Pleistocene to Early Holocene evolution of barrier-lagoon systems on the northern Adriatic shelf (Italy). *Quat. Sci. Rev.* **2008**, *27*, 1107–1123. [CrossRef]
7. Green, A.N.; Cooper, J.A.G.; Leuci, R.; Thackeray, R. Formation and preservation of an overstepped segmented lagoon complex on a high-energy continental shelf. *Sedimentology* **2013**, *60*, 1755–1768. [CrossRef]
8. Pretorius, L.; Green, A.N.; Cooper, J.A.G.; Hahn, A.; Zabel, M. Outer- to inner-shelf response to stepped sea-level rise: Insights from incised valleys and submerged shorelines. *Mar. Geol.* **2019**, *416*, 105979. [CrossRef]
9. Billy, J.; Robin, N.; Hein, C.J.; FitzGerald, D.M.; Certain, R. Impact of relative sea-level changes since the last deglaciation on the formation of a composite paraglacial barrier. *Mar. Geol.* **2018**, *400*, 76–93. [CrossRef]
10. Billy, J.; Robin, N.; Hein, C.J.; Certain, R.; FitzGerald, D.M. Insight into the late Holocene sea-level changes in the NW Atlantic from a paraglacial beach-ridge plain south of Newfoundland. *Geomorphology* **2015**, *248*, 134–146. [CrossRef]
11. Wang, R.; Colombera, L.; Mountney, N.P. Geological controls on the geometry of incised-valley fills: Insights from a global dataset of late-Quaternary examples. *Sedimentology* **2019**, *66*, 2134–2168. [CrossRef]
12. Maselli, V.; Trincardi, T.; Asioli, A.; Ceregato, A.; Rizzetto, F.; Taviani, M. Delta growth and river valleys: The influence of climate and sea level changes on the South Adriatic shelf (Mediterranean Sea). *Quat. Sci. Rev.* **2014**, *99*, 146–163. [CrossRef]
13. Maselli, V.; Hutton, E.W.; Kettner, A.J.; Syvitski, J.P.M.; Trincardi, F. High-frequency sea level and sediment supply fluctuations during Termination I: An integrated sequence-stratigraphy and modeling approach from the Adriatic Sea (Central Mediterranean). *Mar. Geol.* **2011**, *287*, 54–70. [CrossRef]
14. Trincardi, F.; Cattaneo, A.; Asioli, A.; Correggiari, A.; Langone, L. Stratigraphy of the Late-Quaternary deposits in the central Adriatic basin and the record of short term climatic events. *Mem. Ist. Ital. Idrobiol.* **1996**, *55*, 39–70.
15. Berné, S.; Jouet, G.; Bassetti, M.A.; Dennielou, B.; Taviani, M. Late Glacial Preboreal sea-level rise recorded by the Rhône deltaic system (NW Mediterranean). *Mar. Geol.* **2007**, *245*, 65–88. [CrossRef]
16. Caldara, M.; Pennetta, L. Pleistocenic buried abrasion platforms in southeastern "Tavoliere" (Apulia, South Italy). *Alp. Mediterr. Quat.* **1991**, *4*, 303–309.
17. Caldara, M.; Iannone, A.; Lopez, R.; Simone, O.; De Santis, V.; Torres, T.; Ortiz, J.E. New data on the Pleistocene of Trani (Adriatic coast, southern Italy). *Ital. J. Geosci.* **2013**, *132*, 239–253. [CrossRef]
18. De Santis, V.; Caldara, M.; Torres, T.; Ortiz, J.E. Stratigraphic units of the Apulian Tavoliere Plain: Chronology, correlation with marine isotope stages and implication regarding vertical movements. *Sediment. Geol.* **2010**, *228*, 255–270. [CrossRef]
19. De Santis, V.; Caldara, M.; Pennetta, L.; Torres, T.; Ortiz, J.E. Unconformity bounded stratigraphic units in an Italian alluvial plain area: Recognising and dating. *J. Sediment. Res.* **2013**, *83*, 96–114. [CrossRef]
20. De Santis, V.; Caldara, M.; Pennetta, L. The marine and alluvial terraces of Tavoliere di Puglia plain (southern Italy). *J. Maps* **2014**, *10*, 114–125. [CrossRef]
21. De Santis, V.; Caldara, M.; Torres, T.; Ortiz, J.E. Two middle Pleistocene warm stages in the terraced deposits of the Apulia region (southern Italy). *Quat. Int.* **2014**, *332*, 2–18. [CrossRef]
22. De Santis, V.; Caldara, M.; Torres, T.; Ortiz, J.E.; Sánchez-Palencia, Y. A review of MIS 7 and MIS 5 terrace deposits along the Gulf of Taranto based on new stratigraphic and chronological data. *Ital. J. Geosci.* **2018**, *137*, 349–368. [CrossRef]
23. De Santis, V.; Caldara, M.; Torres, T.; Ortiz, J.E.; Sánchez-Palencia, Y. The role of beach ridges, spits, or barriers in understanding marine terraces processes on loose or semiconsolidated substrates: Insights from the givoni of the Gulf of Taranto (Southern Italy). *Geol. J.* **2020**, *55*, 2951–2975. [CrossRef]

24. Fabbri, A.; Gallignani, P. Ricerche geomorfologiche e sedimentologiche nell'Adriatico meridionale. *Giorn Geol.* **1972**, *38*, 453–498.
25. Caldara, M.; Centenaro, E.; Mastronuzzi, G.; Sansò, P.; Sergio, A. Features and present evolution of apulian coast (Southern Italy). *J. Coast. Res.* **1998**, *SI26*, 55–64.
26. De Santis, V.; Caldara, M. The 5.5-4.5 kyr climatic transition as recorded by the sedimentation pattern of coastal deposits of Apulia region, southern Italy. *Holocene* **2015**, *25*, 1313–1329. [CrossRef]
27. De Santis, V.; Caldara, M.; Pennetta, L. Continuous Backstepping of Holocene Coastal Barrier Systems into Incised Valleys: Insights from the Ofanto and Carapelle-Cervaro Valleys. *Water* **2020**, *12*, 1799. [CrossRef]
28. Trincardi, F.; Argnani, A.; Correggiari, A. *Note Illustrative della Carta Geologica dei Mari Italiani, Alla Scala 1:250,00, Foglio NK33-6 Vieste, e Foglio NK33-8/9 Bari*; ISPRA: Roma, Italy, 2011; pp. 1–194.
29. Trincardi, F.; Correggiari, A.; Ridente, D.; Verdicchio, G.; Cattaneo, A.; Minisini, D.; Remia, A.; Taviani, M.; Asioli, A.; Piva, A.; et al. *Carta Geologica dei Mari Italiani, Foglio NK33-8/9 Bari*; ISPRA: Roma, Italy, 2011.
30. Maselli, V.; Trincardi, F. Large-scale single incised valley from a small catchment basin on the western Adriatic margin (central Mediterranean Sea). *Glob. Planet. Chang.* **2013**, *100*, 245–262. [CrossRef]
31. Ridente, R. Late Pleistocene post-glacial sea level rise and differential preservation of transgressive "sand ridges" deposits in the Adriatic sea. *Geosciences* **2018**, *8*, 61. [CrossRef]
32. De Santis, V.; Caldara, M. Evolution of an incised valley system in the southern Adriatic Sea (Apulian margin): An onshore-offshore correlation. *Geol. J.* **2016**, *51*, 263–284. [CrossRef]
33. Catuneanu, O.; Galloway, W.E.; Kendall, C.G.S.T.C.; Miall, A.D.; Posamentier, H.W.; Strasser, A.; Tucker, M.E. Sequence stratigraphy: Methodology and Nomenclature. *Newsl. Stratigr.* **2011**, *44*, 173–245. [CrossRef]
34. Amorosi, A.; Maselli, V.; Trincardi, F. Onshore to offshore anatomy of a late Quaternary source-to-sink system (Po Plain–Adriatic Sea, Italy). *Earth-Sci. Rev.* **2016**, *153*, 212–237. [CrossRef]
35. Cattaneo, A.; Correggiari, A.; Langone, L.; Trincardi, F. The late-Holocene Gargano subaqueous delta, Adriatic shelf: Sediment pathways and supply fluctuations. *Mar. Geol.* **2003**, *193*, 61–91. [CrossRef]
36. Cattaneo, A.; Trincardi, F. The late-Quaternary transgressive record in the Adriatic epicontinental sea: Basin widening and facies partitioning. In *Isolated Shallow Marine Sand Bodies: Sequence Stratigraphic Analysis and Sedimentologic Interpretation*; Bergman, K., Snedden, J., Eds.; SEPM: Broken Arrow, OK, USA, 1999; Volume 64, pp. 127–146.
37. Correggiari, A.; Trincardi, F.; Langone, L.; Roveri, M. Styles of failure in heavily-sedimented highstand prodelta wedges on the Adriatic shelf. *J. Sediment. Res.* **2001**, *71*, 218–236. [CrossRef]
38. Pellegrini, C.; Maselli, V.; Cattaneo, A.; Piva, A.; Ceregato, A.; Trincardi, F. Anatomy of a compound delta from the post-glacial transgressive record in the Adriatic Sea. *Mar. Geol.* **2015**, *362*, 43–59. [CrossRef]
39. Cooper, J.A.G.; Green, A.N.; Meireles, R.P.; Klein, A.H.F.; Souza, J.; Toldo, E.E. Sandy barrier overstepping and preservation linked to rapid sea level rise and geological setting. *Mar. Geol.* **2016**, *382*, 80–91. [CrossRef]
40. Esker, D.; Eberli, G.P.; McNeill, D.F. The Structural and Sedimentological Controls on the Reoccupation of Quaternary Incised Valleys, Belize Southern Lagoon. *AAPG Bull.* **1998**, *82*, 2075–2109.
41. Labaune, C.; Tesson, M.; Gensous, B.; Parize, O.; Imbert, P.; Delhaye-Prat, V. Detailed architecture of a compound incised valley system and correlation with forced regressive wedges: Example of Late Quaternary Têt and Agly rivers, western Gulf of Lions, Mediterranean Sea, France. *Sediment. Geol.* **2010**, *223*, 360–379. [CrossRef]
42. Maio, C.V.; Gontz, A.M.; Sullivan, R.M.; Madsen, S.M.; Weidman, C.R.; Donnelly, J.P. Subsurface evidence of storm-driven breaching along a transgressing barrier system, Cape Cod, U.S.A. *J. Coast. Res.* **2015**, *32*, 264–279. [CrossRef]
43. Nordfjord, S.; Goff, J.A.; Austin, J.A., Jr.; Gulick, S.P.S. Seismic facies of incised-valley fills, New Jersey continental shelf: Implications for erosion and preservation processes acting during latest Pleistocene-Holocene transgression. *J. Sediment. Res.* **2006**, *76*, 1284–1303. [CrossRef]
44. Raynal, O.; Bouchette, F.; Certain, R.; Sabatier, P.; Lofi, J.; Séranne, M.; Dezileau, L.; Briqueu, L.; Ferrer, P.; Courp, T. Holocene evolution of a Languedocian lagoonal environment controlled by inherited coastal morphology (northern Gulf of Lions, France). *Bull. Soc. Geol. Fr.* **2010**, *181*, 211–224. [CrossRef]
45. Lambeck, K.; Antonioli, F.; Anzidei, M.; Ferranti, L.; Leoni, G.; Silenzi, S. Sea level change along the Italian coasts during Holocene and prediction for the future. *Quat. Int.* **2011**, *232*, 250–257. [CrossRef]
46. Lambeck, K.; Rouby, H.; Purcell, A.; Sun, Y.; Sambradge, M. Sea level and global ice volumes from the Last Glacial Maximum to the Holocene. *Proc. Natl. Acad. Sci. USA* **2014**, *111*, 15296–15303. [CrossRef] [PubMed]

47. Liu, J.P.; Milliman, J.D. Reconsidering melt-water pulses 1A and 1B: Global impacts of rapid sea-level rise. *J. Ocean Univ. China* **2004**, *3*, 183–190. [CrossRef]
48. Bard, E.; Hamelin, B.; Delanghe-Sabatier, D. Deglacial meltwater pulse 1B and younger dryas sea levels revisited with Boreholes at Tahiti. *Science* **2010**, *327*, 1235–1237. [CrossRef] [PubMed]
49. Zecchin, M.; Ceramicola, S.; Gordini, E.; Deponte, M.; Critelli, S. Cliff overstep model and variability in the geometry of transgressive erosional surfaces in high-gradient shelves: The case of the Ionian Calabrian margin (Southern Italy). *Mar. Geol.* **2011**, *281*, 43–58. [CrossRef]
50. Zecchin, M.; Gordini, E.; Ramella, M. Recognition of a drowned delta in the northern Adriatic Sea, Italy: Stratigraphic characteristics and its significance in the frame of the early Holocene sea-level rise. *Holocene* **2015**, *25*, 1027–1038. [CrossRef]
51. Civile, D.; Lodolo, E.; Zecchin, M.; Ben-Avraham, Z.; Baradello, L.; Accettella, D.; Cova, A.; Caffau, M. The lost Adventure Archipelago (Sicilian Channel, Mediterranean Sea): Morpho-bathymetry and Late Quaternary palaeogeographic evolution. *Glob. Planet. Chang.* **2015**, *125*, 36–47. [CrossRef]
52. Caldara, M.; Capolongo, D.; Del Gaudio, V.; De Santis, V.; Pennetta, L.; Maiorano, P.; Simone, O.; Vitale, G. *Note Illustrative della Carta Geologica d'Italia alla Scala 1:50.000 Foglio, 422 "Cerignola"*; Istituto Superiore per la Protezione e la Ricerca Ambientale: Roma, Italy, 2011; pp. 1–96. ISBN 978-88-240-2989-6.
53. Caldara, M.; Capolongo, D.; Del Gaudio, V.; De Santis, V.; Pennetta, L.; Maiorano, P.; Simone, O. *Note Illustrative della Carta Geologica d'Italia alla Scala 1:50.000 Foglio, 409 "Zapponeta"*; Istituto Superiore per la Protezione e la Ricerca Ambientale: Roma, Italy, in press.
54. Boenzi, F.; Caldara, M.; Pennetta, L.; Simone, O. Environmental aspects related to the physical evolution of some wetlands along the Adriatic coast of Apulia (Southern Italy): A review. *J. Coast. Res.* **2006**, *SI39*, 170–175.
55. Strong, N.; Paola, C. Fluvial landscapes and stratigraphy in a flume. *Sediment. Rec.* **2006**, *4*, 4–8. [CrossRef]
56. Strong, N.; Paola, C. Valleys that never were: Time surfaces versus stratigraphic surfaces. *J. Sediment. Res.* **2008**, *78*, 579–593. [CrossRef]
57. Schumm, S.A.; Brackenridge, S.A. River response. In *North America and Adjacent Oceans during the Last Deglaciation*; Ruddiman, W.F., Wright, H.E., Jr., Eds.; Geological Society of America, The Geology of North America: Boulder, CO, USA, 1987; pp. 221–240.
58. Leckie, D.A. Canterbury Plains, New Zealand–implications for sequence stratigraphic models. *AAPG Bull.* **1994**, *78*, 1240–1256. [CrossRef]
59. Posamentier, H.W. Lowstand alluvial bypass systems: Incised vs unincised. *Am. Assoc. Pet. Geol. Bull.* **2001**, *85*, 1771–1793. [CrossRef]
60. Posamentier, H.W.; Allen, G.P. Siliciclastic Sequence Stratigraphy: Concepts and Applications. In *SEPM Concepts in Sedimentology and Paleontology*; Society for Sedimentary Geology: Tulsa, OK, USA, 1999; Volume 7, pp. 1–210.
61. Paola, C.; Heller, P.L.; Angevine, C.L. The largescale dynamics of grain-size variation in alluvial basins, 1: Theory. *Basin Res.* **1992**, *4*, 73–90. [CrossRef]
62. Blum, M.; Martin, J.; Milliken, K.; Garvin, M. Paleovalley systems: Insights from Quaternary analogs and experiments. *Earth-Sci. Rev.* **2013**, *116*, 128–169. [CrossRef]
63. Van Heijst, M.W.I.M.; Postma, G. Fluvial response to sea-level changes: A quantitative analogue, experimental approach. *Basin Res.* **2001**, *13*, 269–292. [CrossRef]
64. Loget, N.; Van Den Driessche, J. Wave train model for knickpoint migration. *Geomorphology* **2009**, *106*, 376–382. [CrossRef]
65. Makinouchi, T.; Mori, S.; Danhara, T.; Takemura, K. Stratigraphic horizon and formational process of the First Gravel Formation (BG) in the Nohbi Plain. In Recent Progress on the Understanding of So-called Chuseki-so. *Mem. Geol. Surv. Jpn.* **2006**, *59*, 129–139.
66. Ishihara, T.; Sugai, T.; Hachinohe, S. Fluvial response to sea-level changes since the latest Pleistocene in the near-coastal lowland, central Kanto Plain, Japan. *Geomorphology* **2012**, *147–148*, 49–60. [CrossRef]
67. Ishihara, T.; Sugai, T. Eustatic and regional tectonic controls on late Pleistocene paleovalley morphology in the central Kanto Plain. *Jpn. Quat. Int.* **2017**, *456*, 69–84. [CrossRef]
68. Blum, M.D.; Tornqvist, T.E. Fluvial responses to climate and sea-level change: A review and look forward. *Sedimentology* **2000**, *47*, 2–48. [CrossRef]
69. Mattheus, C.R.; Rodriguez, A.B.; Greene, D.L.; Simms, A.R.; Anderson, J.B. Control of upstream variables on incised-valley dimension. *J. Sediment. Res.* **2007**, *77*, 213–224. [CrossRef]

70. Mattheus, C.R.; Rodriguez, A.B. Controls on late Quaternary incised-valley dimension along passive margins evaluated using empirical data. *Sedimentology* **2011**, *58*, 1113–1137. [CrossRef]
71. Phillips, J.D. Drainage area and incised valley fills in Texas rivers: A potential explanation. *Sediment. Geol.* **2011**, *242*, 65–70. [CrossRef]
72. Blum, M.D.; Womack, J.H. Climate change, sea level change, and fluvial sediment supply to deepwater systems. In *External Controls on Deep Water Depositional Systems: Climate, Sea-Level, and Sediment Flux*; Kneller, B., Martinsen, O.J., McCaffrey, B., Eds.; SEPM: Broken Arrow, OK, USA, 2009; Volume 92, pp. 15–39, Special Publication.
73. Patruno, S.; Hampson, G.J.; Jackson, C.A.-L. Quantitative characterisation of deltaic and subaqueous clinoforms. *Earth-Sci. Rev.* **2015**, *142*, 79–119. [CrossRef]
74. Cattaneo, A.; Trincardi, F.; Asioli, A.; Correggiari, A. The western Adriatic shelf clinoform: Energy-limited bottomset. *Cont. Shelf Res.* **2007**, *27*, 506–525. [CrossRef]
75. Correggiari, A.; Cattaneo, A.; Trincardi, F. The modern Po Delta system: Lobe switching and asymmetric prodelta growth. *Mar. Geol.* **2005**, *222–223*, 49–74. [CrossRef]
76. Engelbrecht, L.; Green, A.N.; Cooper, J.A.G.; Hahn, A.; Zabel, M.; Mackay, C.F. Construction and evolution of submerged deltaic bodies on the high energy SE African coastline: The interplay between relative sea level and antecedent controls. *Mar. Geol.* **2020**, *424*, 106170. [CrossRef]
77. Stanford, J.D.; Hemingway, R.; Rohling, E.J.; Challenor, P.G.; Medina-Elizalde, M.; Lester, A.J. Sea-level probability for the last deglaciation: A statistical analysis of far-field records. *Glob. Planet. Chang.* **2011**, *79*, 193–203. [CrossRef]
78. Sømme, T.O.; Piper, D.J.W.; Deptuck, M.E.; Helland-Hansen, W. Linking Onshore–Offshore sediment dispersal in the Golo source-to-sink system (Corsica, France) during the Late Quaternary. *J. Sediment. Res.* **2011**, *81*, 118–137. [CrossRef]
79. Green, A.N.; Cooper, J.A.G.; Salzmann, L. Geomorphic and stratigraphic signals of postglacial meltwater pulses on continental shelves. *Geology* **2014**, *24*, 151–154. [CrossRef]
80. Ariztegui, D.; Asioli, A.; Lowe, J.J.; Trincardi, F.; Vigliotti, L.; Tamburini, F.; Chondrogianni, C.; Accorsi, C.A.; Bandini Mazzanti, M.; Mercuri, A.M.; et al. Palaeoclimate and the formation of sapropel S1: Inferences from Late Quaternary lacustrine and marine sequences in the central Mediterranean region. *Palaeogeogr. Palaeoclimatol. Palaeoecol.* **2000**, *158*, 215–240. [CrossRef]
81. Tesi, T.; Asioli, A.; Minisini, D.; Maselli, V.; Dalla Valle, G.; Gamberi, F.; Langone, L.; Cattaneo, A.; Montagna, P.; Trincardi, F. Large-scale response of the Eastern Mediterranean thermohaline circulation to African monsoon intensification during sapropel S1 formation. *Quat. Sci. Rev.* **2017**, *159*, 139–154. [CrossRef]
82. Cronin, T.M.; Vogt, P.R.; Willard, D.A.; Thunell, R.C.; Halka, J.; Berke, M.; Pohlman, J. Rapid sea level rise and ice sheet response to 8200-year climate event. *Geophys. Res. Lett.* **2007**, *34*. [CrossRef]
83. Hijma, M.P.; Coen, K.M. Timing and magnitude of the sea-level jump preluding the 8200 yr event. *Geology* **2010**, *38*, 275–278. [CrossRef]
84. Rampino, M.R.; Sanders, J.E. Holocene transgression in south-central Long Island, New York. *J. Sediment. Petrol.* **1980**, *50*, 1063–1080.
85. Sanders, J.E.; Kumar, N. Evidence of shoreface retreat and in-place "drowning" during Holocene submergence of barriers, shelf off Fire Island, New York. *Geol. Soc. Am. Bull.* **1975**, *86*, 65–76. [CrossRef]
86. Cooper, J.A.G.; Green, A.N.; Compton, J.S. Sea-level change in southern Africa since the Last Glacial Maximum. *Quat. Sci. Rev.* **2018**, *201*, 303–318. [CrossRef]